CORRECTED 12 JANUARY 2022; SEE ERRATUM

SCIENCE TRANSLATIONAL MEDICINE | RESEARCH ARTICLE

ALZHEIMER'S DISEASE

The *Uppsala APP* deletion causes early onset autosomal dominant Alzheimer's disease by altering APP processing and increasing amyloid β fibril formation

María Pagnon de la Vega[1], Vilmantas Giedraitis[1], Wojciech Michno[2,3], Lena Kilander[1], Gökhan Güner[4], Mara Zielinski[5], Malin Löwenmark[1], RoseMarie Brundin[1], Torsten Danfors[6], Linda Söderberg[7], Irina Alafuzoff[8], Lars N.G. Nilsson[9], Anna Erlandsson[1], Dieter Willbold[5,10,11], Stephan A. Müller[4], Gunnar F. Schröder[5,12], Jörg Hanrieder[2,13], Stefan F. Lichtenthaler[4,14], Lars Lannfelt[1], Dag Sehlin[1†], Martin Ingelsson[1*†]

Point mutations in the amyloid precursor protein gene (*APP*) cause familial Alzheimer's disease (AD) by increasing generation or altering conformation of amyloid β (Aβ). Here, we describe the *Uppsala APP* mutation (Δ690–695), the first reported deletion causing autosomal dominant AD. Affected individuals have an age at symptom onset in their early forties and suffer from a rapidly progressing disease course. Symptoms and biomarkers are typical of sporadic AD, except that these three patients had high cerebrospinal fluid (CSF) Aβ42 and only modest brain pathology as detected by amyloid-positron emission tomography. Mass spectrometry and Western blot analyses of patient CSF and media from experimental cell cultures indicate that the *Uppsala APP* mutation alters APP processing by increasing β-secretase cleavage and affecting α-secretase cleavage. Furthermore, in vitro aggregation studies and analyses of patient brain tissue samples indicate that the longer form of mutated Aβ, AβUpp1–42$_{\Delta 19-24}$, accelerates the formation of fibrils with unique polymorphs and their deposition into amyloid plaques in the affected brain.

INTRODUCTION

Alzheimer's disease (AD) is neuropathologically characterized by a progressive deposition of amyloid β (Aβ) in parenchyma and blood vessels of the cerebrum (*1*). Upon sequential cleavage of the amyloid precursor protein (APP) by β- and γ-secretases, Aβ peptides of 38 to 43 amino acids are generated. If instead α-secretase cleavage occurs, then no Aβ is formed [reviewed in (*2*)].

Increased generation of the more amyloidogenic Aβ42 is seen for several of the *APP* mutations positioned in vicinity of the γ-secretase cleavage site (*3*–*14*), whereas the *Swedish* mutation close to the β-secretase cleavage site results in increased production of both Aβ42 and Aβ40, as demonstrated in plasma and fibroblasts from mutation carriers (*15*–*17*). Pathogenic *APP* mutations within the Aβ sequence have been described to result in various disease phenotypes. Patients with the *Dutch* (E693Q) and *Italian* (E693K) mutations display amyloid accumulation in cerebral blood vessel walls and intracerebral hemorrhage (*18*, *19*), whereas carriers of the *Flemish* (A692G) and *Iowa* (D694N) mutations suffer from both intracerebral hemorrhage and progressive dementia (*20*, *21*). The *Arctic* mutation (E693G) leads to an increased formation of protofibrils (*22*) and other large Aβ oligomers with particularly neurotoxic properties (*23*). Clinical examinations and neuropathological analyses confirmed that carriers of the *Arctic* mutation have an AD phenotype (*24*), although their brains almost only display diffuse parenchymal Aβ deposits (*24*–*26*). The only protective *APP* variant described to date, the *Icelandic* mutation (A673T), has been shown to decrease β-secretase cleavage resulting in reduced Aβ production (*27*) and aggregation (*28*, *29*).

For the only identified disease-causing *APP* deletion (E693Δ), resulting in a recessive form of familial AD, an increased intraneuronal presence of toxic Aβ oligomers was suggested as an underlying pathogenic feature. A decreased inhibition of both β- and γ-secretase, with increased enzymatic activities and relative resistance to degradation of mutant Aβ by neprilysin and insulin-degrading enzyme, has been proposed as other effects of this deletion (*30*).

Here, we report a pathogenic *APP* deletion (690–695Δ) that causes a dominantly inherited form of early onset dementia in three mutation carriers of a family originating from the city of Uppsala, Sweden. Clinical and neuropathological examinations are compatible with AD, and experimental studies indicate that the phenotype is caused by pathological alterations of the β- and α-secretase cleavage of APP, which result in increased Aβ production in combination with a very rapid aggregation of the longer Aβ mutant (AβUpp1–42$_{\Delta 19-24}$) into unique polymorphic structures.

[1]Department of Public Health and Caring Sciences, Geriatrics, Uppsala University, 75185 Uppsala, Sweden. [2]Department of Psychiatry and Neurochemistry, University of Gothenburg, 43180 Gothenburg, Sweden. [3]Department of Neuroscience, Physiology and Pharmacology, University College London, WC1E 6BT London, UK. [4]German Center for Neurodegenerative Diseases (DZNE) and Neuroproteomics, School of Medicine, Klinikum rechts der Isar, Technical University of Munich, 81377 Munich, Germany. [5]Institute of Biological Information Processing, Structural Biochemistry (IBI-7) and JuStruct, Jülich Center for Structural Biology, Forschungszentrum Jülich, 52425 Jülich, Germany. [6]Department of Surgical Sciences, Radiology, Uppsala University, 75185 Uppsala, Sweden. [7]BioArctic AB, 11251 Stockholm, Sweden. [8]Department of Immunology, Genetics and Pathology, Clinical and Experimental Pathology, Uppsala University, 75185 Uppsala, Sweden. [9]Department of Pharmacology, University of Oslo and Oslo University Hospital, 0316 Oslo, Norway. [10]Institut für Physikalische Biologie, Heinrich-Heine-Universität Düsseldorf, 40225 Düsseldorf, Germany. [11]Research Center for Molecular Mechanisms of Aging and Age-Related Diseases, Moscow Institute of Physics and Technology, State University, 141701 Dolgoprudny, Russia. [12]Physics Department, Heinrich-Heine-Universität Düsseldorf, 40225 Düsseldorf, Germany. [13]Department of Neurodegenerative Disease, Queen Square Institute of Neurology, University College London, WC1N 3BG London, UK. [14]Munich Cluster for Systems Neurology (SyNergy), 81377 Munich, Germany.
*Corresponding author. Email: martin.ingelsson@pubcare.uu.se
†These authors contributed equally to this work.

RESULTS

Epidemiological and clinical features of the *Uppsala APP* mutation family

The *Uppsala APP* mutation was detected in two siblings and their cousin, who were all referred to the Memory Disorder Unit, Uppsala University Hospital (for pedigree, see Fig. 1A). The ages of symptom onset were 43 years (sibling 1), 40 years (sibling 2), and 41 years (cousin). All three patients had a manifest cognitive impairment and scored 20 to 22 points on the Mini-Mental State Examination (MMSE) at the time of referral, with word finding difficulties, dyscalculia, apraxia, and visuospatial/executive impairment as major symptoms. Sibling 1 developed myoclonus and had a rapid disease progression with severe anxiety and behavioral disturbances. Death occurred 6 years after onset, at the age of 49. At the initial neuropsychological evaluation, sibling 2 had normal scores on episodic memory tests but featured severe dyscalculia and problems with the clock drawing test. At the 4-year follow-up examination, this patient had become increasingly affected by apathy and mutism. The cousin of the two siblings displayed impaired episodic memory, language, and executive functions as dominant symptoms.

One parent of the two siblings had been referred for assessment more than 20 years earlier after having refused to see a physician for several years. This patient had symptom onset at about 47 years of age, and the diagnosis of AD was supported by a computerized tomography (CT) scan, showing cortical and central atrophy at the age of 54. Death occurred at the age of 60. One of the parents of the cousin had onset of symptoms at about 45 years of age and was subsequently also diagnosed with AD. This patient became aggressive and spent several years at a geropsychiatric ward before death occurred about 15 years later. In addition, one of the siblings' grandparents developed dementia with onset at about 40 years of age and died at the age of 51 (Fig. 1A).

All three cases underwent lumbar puncture and subsequent cerebrospinal fluid (CSF) analyses. CSF concentrations of Aβ42 were within the normal range of non-AD controls, whereas concentrations of total tau (t-tau) and phospho-tau (p-tau) were pathologically elevated (table S1).

Brain imaging

The two siblings and their cousin underwent CT brain examinations at the time of diagnosis. The scan of sibling 1, who was in a more advanced disease stage at the initial visit, showed medial temporal lobe atrophy (MTA) grade 2 together with a moderate frontoparietal lobe atrophy. Sibling 2 and his cousin had a moderate global cortical and central atrophy, whereas the temporal lobes were well preserved (MTA grades 0 to 1) (Fig. 1B). Moreover, the siblings and their cousin underwent fluorodeoxyglucose positron emission tomography [^{18}F]FDG-PET, which showed a decreased uptake mainly

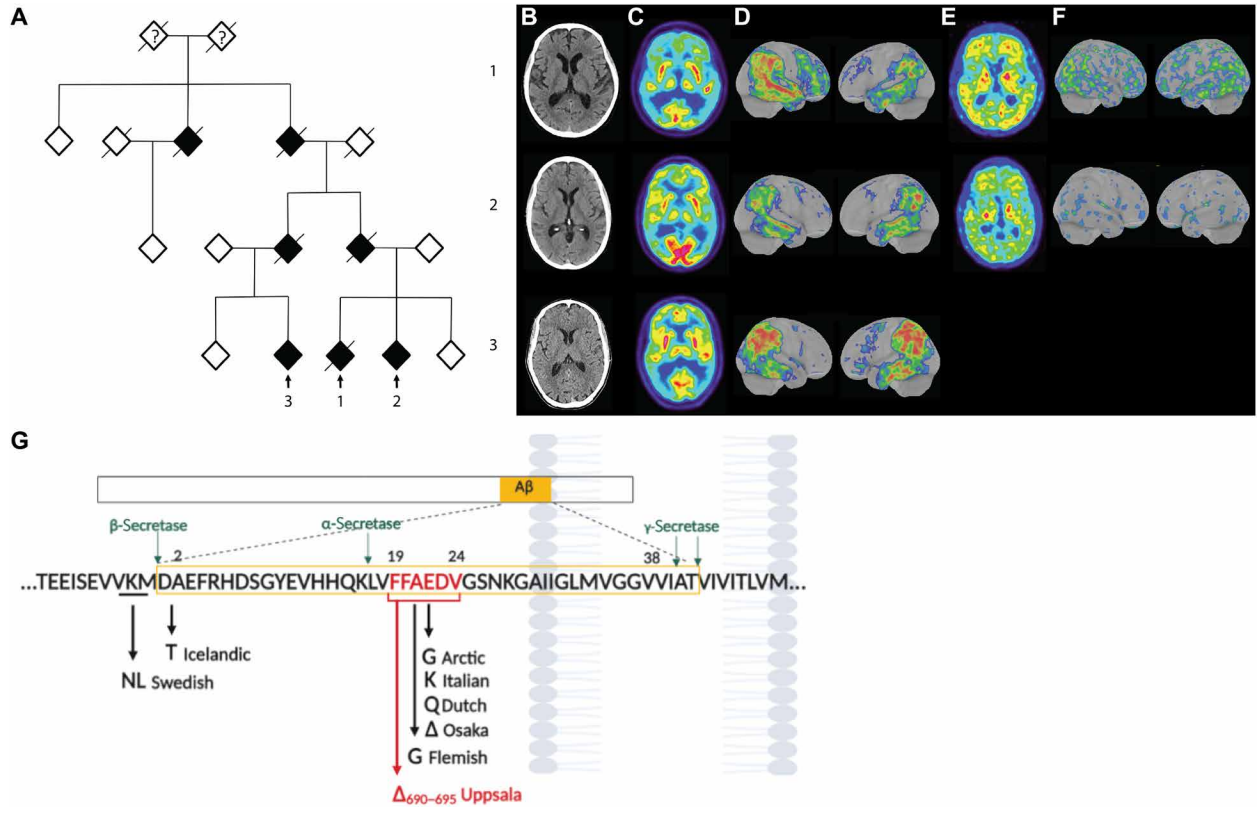

Fig. 1. Epidemiological and clinical features of the *Uppsala APP* mutation family. Pedigree of the *Uppsala APP* mutation family (**A**). Filled symbols are affected family members. Slashed symbols are deceased individuals. Index cases are indicated by arrows. Several healthy individuals in the latest generation have been omitted on purpose. CT and PET images of the three affected patients (sibling 1, sibling 2, and cousin 3, from top to bottom rows). Axial CT (**B**), [^{18}F]FDG-PET (**C** and **D**), and [^{11}C]PIB-PET images (**E** and **F**). Three-dimensional surface projection showing areas with pathological cortical tracer uptake (D and F). For (C) and (D), the color scale represents decreased tracer uptake with *z* score between 0 (blue) and −7 (red). For (E) and (F), the color scale represents increased tracer uptake with *z* scores between 0 (blue) and 8 (red). The location of the *Uppsala APP* mutation and its relation to other intra-Aβ *APP* mutations (**G**).

in the temporal and parietal lobes (Fig. 1, C and D). Two of them also underwent amyloid-PET using Pittsburgh compound B ([^{11}C]PIB), which demonstrated a pathological pattern but only with a slightly increased accumulation of [^{11}C]PIB in cortical areas (Fig. 1, E and F).

Genetic analyses reveal the *Uppsala APP* mutation

In the three affected cases (two siblings and their cousin), we identified an 18–base pair deletion in exon 17, which leads to the loss of six amino acids (690–695Δ) within Aβ. It should be noted that this deletion spans over the region that is affected by previously identified intra-Aβ mutations (Fig. 1G). In addition, we have analyzed more than 500 DNA samples from Swedish patients with AD, older unaffected family members, and from older healthy control subjects, all of which were negative for this genetic alteration. Furthermore, the two siblings were analyzed for the apolipoprotein E gene (*APOE*) and found to be *APOE ε3* homozygotes (table S1).

The *Uppsala APP* mutation leads to mainly AβUpp1–42$_{Δ19–24}$ pathology

One brain of an *Uppsala APP* mutation carrier (sibling 1) has come to autopsy. The weight of the brain was 1480 g, and the right hemisphere was subjected to routine analyses. On gross inspection, dilated ventricles were evident. Microscopically, a pronounced gliosis was seen in limbic and in neocortical areas (Fig. 2A and fig. S1). Moreover, there was a widespread tau pathology, corresponding to Braak stage VI, as visualized with the AT8 anti-tau antibody (Fig. 2, B and C).

Aβ plaques were abundant and widespread, corresponding to Thal stage 5. Tissue sections from occipital (Fig. 2), temporal, and parietal (fig. S1) neocortices were analyzed by immunohistochemistry with a panel of different monoclonal anti-Aβ antibodies and by thioflavin S (ThS) staining. Antibodies directed toward the Aβ C terminus revealed abundant Aβ42 staining, whereas Aβ40 staining was much less intense in all cortical areas investigated (Fig. 2, D to G, and fig. S1). With the 6F/3D antibody, binding to Aβ amino acids 8 to 17 (*25*), abundant pathology was observed in several neocortical regions (Fig. 2H), and a similar pattern could be observed with ThS (Fig. 2I).

Furthermore, brain tissues from fresh-frozen frontal, temporal, and occipital neocortex as well as cerebellum of the mutation carrier, 11 sporadic AD (sAD), and 9 non-neurological control brains (table S2) were homogenized and sequentially extracted with tris-buffered saline (TBS) and formic acid (FA) for analysis with MSD electrochemiluminescence-based Aβ immunoassay (Meso Scale Discovery) and enzyme-linked immunosorbent assay (ELISA). Compared to sAD and control samples, the *Uppsala APP* mutation brain displayed lower concentrations of Aβ40, whereas concentrations of Aβ42 were elevated, especially in the FA fraction (Fig. 3A), which corresponds to insoluble Aβ deposits, but also in the TBS fraction, representing more soluble Aβ, including aggregates (Fig. 3B). In contrast to elevated Aβ42 in the FA fraction of all investigated brain regions, concentrations of TBS soluble oligomers were lower in the *Uppsala APP* mutation brain compared to sAD, when analyzed with an ELISA that detects soluble Aβ aggregates of all sizes (Fig. 3C). Furthermore, when analyzed with an ELISA that preferentially recognizes larger oligomers and protofibrils (*31*), the *Uppsala APP* mutation brain displayed low concentrations, comparable to those in the controls, whereas the amounts of such Aβ species in sAD brains were elevated (Fig. 3D).

The composition of amyloid plaques from temporal neocortex was further analyzed by luminescent conjugated oligothiophene (LCO) staining and matrix-assisted laser desorption/ionization (MALDI) imaging mass spectrometry (IMS). Similar to those that were positive for ThS, plaques stained with the LCOs q-FTAA and h-FTAA (Fig. 3E) showed a distinct core surrounded by a diffuse halo of fibrillar Aβ (Fig. 3F). The MALDI-IMS analyses suggested that the plaques mainly consist of AβUpp42$_{Δ19–24}$, either in its full-length version or as N-terminally truncated peptides, which mainly start at positions 3 (pyroglutamate), 4, 5, or 8. The contribution by AβUpp1–40$_{Δ19–24}$, Aβwt1–40, and Aβwt1–42 to the formation of amyloid plaques in the *Uppsala APP* mutation brain seemed to be minor (Fig. 3, G and H). These results, as well as the peptide sequence identity, were confirmed by immunoprecipitation (IP) and MS analyses of pooled material from 50 individually laser-microdissected plaques, identified with LCO staining (table S3).

To investigate the contribution of AβUpp and Aβwt in CSF from *Uppsala APP* mutation cases and thereby understand why Aβ1–42

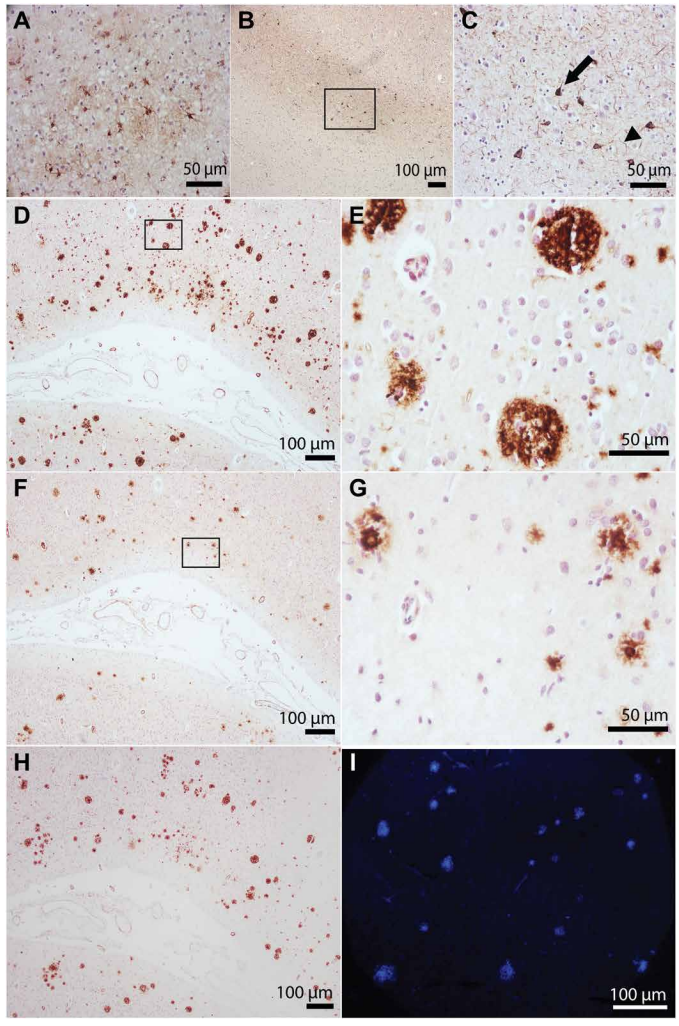

Fig. 2. Pronounced Aβ and tau pathology in the *Uppsala APP* mutation carrier brain. Immunohistochemistry of tissue sections from the *Uppsala APP* mutation brain, against GFAP (glial fibrillary acidic protein) (anti-GFAP) (**A**), tau (AT8) (**B** and **C**), Aβ42 (anti-Aβ42) (**D** and **E**), Aβ40 (anti-Aβ40) (**F** and **G**), and total Aβ (6F/3D) (**H**). Staining of amyloid plaques with ThS (**I**). (A) Temporal cortex; (B to I) occipital cortex. Squares in (B), (D), and (F): Regions displayed in the higher-magnification images (C, E, and G). Arrow in (C) points to a tangle; arrowhead points to a dystrophic neurite.

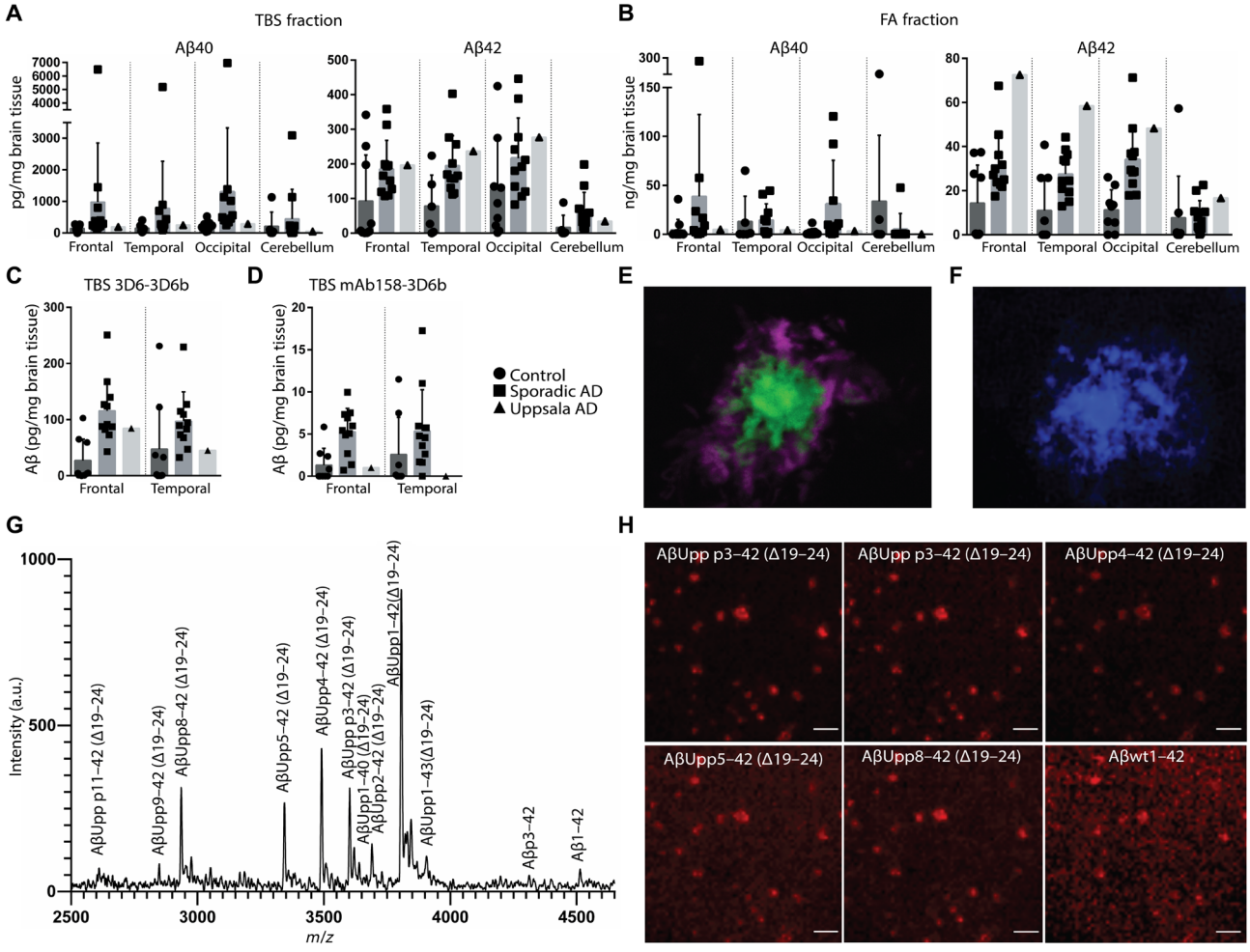

Fig. 3. Plaques in the *Uppsala APP* mutation brain mainly consist of AβUpp42$_{Δ19–24}$. Electrochemiluminescence (MSD) immunoassay (**A** and **B**) and ELISA (**C** and **D**) analyses of human brain extracts. Concentrations of Aβ40 and Aβ42 in the TBS (A) and FA (B) fractions. Concentrations of TBS soluble Aβ aggregates (C) and large Aβ oligomers (D). Staining of Aβ plaques on fresh-frozen temporal neocortical tissue of the *Uppsala APP* mutation brain with the luminescent conjugated oligothiophenes (LCOs) q-FTAA (green) and h-FTAA (purple) (**E**) and with ThS (blue) (**F**). MALDI-IMS spectrum (**G**) and images of plaques from the *Uppsala APP* mutation brain (**H**). Error bars represent SD. For controls, $n = 9$; for sporadic AD (sAD), $n = 11$. Because $n = 1$ for the Uppsala AD group, no statistical analysis was performed. a.u., arbitrary units; *m/z*, mass/charge ratio.

CSF concentrations were within the normal range in these patients, we performed IP-MS analyses using 6E10 (Aβ amino acids 5 to 10) and antibodies targeting the Aβ40 and Aβ42 C terminus for IP. CSF from the three mutation carriers (sibling 1, sibling 2, and cousin) was analyzed and compared to CSF from 11 sAD cases and 10 healthy control subjects (Fig. 4A) (demographic information; table S1). Mutation carriers displayed higher CSF amounts of Aβ1–40, Aβ1–42, and total Aβ (sum of all detected Aβ variants) as compared to sAD cases and control subjects (Fig. 4B). The amounts of Aβwt1–40 and Aβwt1–42 in CSF, produced from the nonmutated *APP* allele, were lower in patients with the *Uppsala APP* mutation compared to healthy control subjects. In addition, the amount of Aβwt1–40 in the CSF of patients with the mutation was lower than in sAD cases (Fig. 4C). The *Uppsala APP* mutation carriers displayed a relative increase of both AβUpp1–40$_{Δ19–24}$ and AβUpp1–42$_{Δ19–24}$ (Fig. 4D). Thus, the expression of Aβ from the mutated allele probably accounts for the unexpectedly high Aβ1–42 CSF concentrations in the routine analysis of patients with the *Uppsala APP* mutation. These measurements were performed with an immunoassay that should detect Aβwt1–42 and AβUpp1–42$_{Δ19–24}$ equally well. However, a comparison of Aβ1–42 measurements performed with the routine immunoassay and IP-MS (fig. S2A) showed that whereas values from control and sAD samples correlated well between the two methods, those from the three *Uppsala APP* mutation cases did not (fig. S2B). Ion spectra from AβUpp1–42$_{Δ19–24}$ and AβUpp1–40$_{Δ19–24}$ are shown in fig. S3.

The *Uppsala APP* mutation alters APP processing, resulting in increased Aβ production

To study the potential effects of the *Uppsala APP* mutation on APP processing, conditioned media of human embryonic kidney (HEK) 293 cells transfected with *APP* carrying the *Uppsala* mutation (*APPUpp*) or wild-type *APP* (*APPwt*) were analyzed with MSD immunoassays to determine sAPPα and sAPPβ concentrations of soluble APP fragments resulting from α- and β-cleavage, as well as in Aβ40 and Aβ42. Only background amounts of sAPPα were detected in media from the *APPUpp* culture, whereas high concentrations were found in media

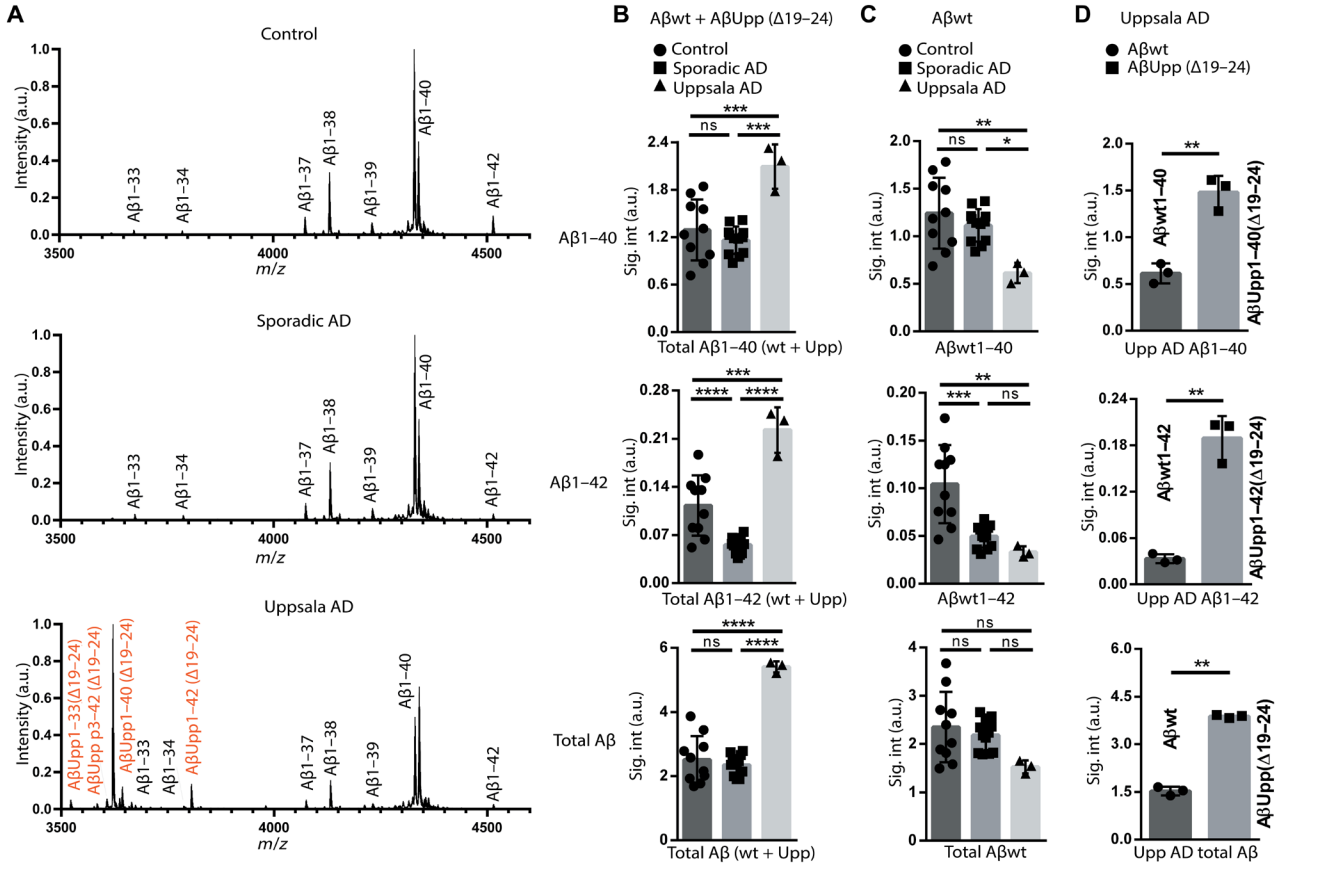

Fig. 4. *Uppsala APP* mutation carriers present increased concentration of Aβ in CSF. IP-MS analyses of CSF from 10 healthy controls, 11 sAD cases, and the 3 *Uppsala APP* mutation patients (**A**). IP-MS–based quantitation of CSF Aβ1–40, Aβ1–42, and total Aβ concentrations in CSF (**B** to **D**). All data are represented as group means, and error bars represent SD. The arbitrary units in the *y* axes represent ratios of intact mass peak area of individual Aβ peptide signals normalized to the spiked Aβ1–40 internal standard. For control CSF, $n = 10$; for sAD, $n = 11$; for Uppsala CSF, $n = 3$. Analyses of individual peptide signals and comparisons between the groups were performed by one-way ANOVA in (B) ($P = 0.0002$, $P < 0.0001$, and $P < 0.0001$ for Aβ1–40, Aβ1–42, and total Aβ, respectively) and (C) ($P = 0.0069$, $P = 0.0001$, and $P = 0.0767$ for Aβ1–40, Aβ1–42, and total Aβ, respectively) followed by Tukey's post hoc test. For (D), paired *t* test was performed ($P = 0.0029$, $P = 0.0081$, and $P = 0.0007$ for Aβ1–40, Aβ1–42, and total Aβ, respectively). Nonsignificant (ns), $^{*}P < 0.05$, $^{**}P < 0.01$, $^{***}P < 0.001$, and $^{****}P < 0.0001$.

from *APPwt*-expressing cells (Fig. 5A). In contrast, concentrations of sAPPβ were higher in media from *APPUpp* than *APPwt* cells (Fig. 5B), which was also reflected in a higher concentration of both Aβ40 and Aβ42 (Fig. 5C).

To study whether the *Uppsala APP* mutation causes an ablation of α-secretase cleavage or whether the cleavage site is shifted toward the N terminus due to the six–amino acid deletion, Western blot was performed on the same cell media as used for the MSD analyses. Total soluble APP (detected with 22C11, binding to an N-terminal epitope of APP) was similar in cell media from *APPUpp*- and *APPwt*-transfected cells. Similar to the MSD analyses, no sAPPα could be detected in the media from the *APPUpp* culture when probing with 6E10 (directed against Aβ amino acids 5 to 10 and usually present on sAPPα) ($P = 0.0004$) or 2B3 (specific for the C-terminal end of sAPPα) ($P = 0.0045$). However, when detected with mAb1C3 that binds to Aβ amino acids 3 to 8, which is closer to the APP N terminus than 6E10 (fig. S4), a faint sAPPα band was observed ($P = 0.0291$) (Fig. 5, D and E).

Next, the same cell media were analyzed with two different Aβ sandwich ELISAs: Aβ1–40 (using Aβ N-terminal–specific antibody 3D6 for detection) and Aβx–40 (using 6E10 for detection). Because the MSD and Western blot–based results suggested an additional cleavage site in *APPUpp* resulting in mAb1C3-positive sAPP fragment, we expected that the C-terminal side of this cleavage site would be detectable with the Aβx–40 ELISA (Fig. 5F). Cell media from the *APPUpp* culture showed a significantly higher ($P = 0.0016$) Aβx–40/Aβ1–40 ratio compared to *APPwt*-transfected cells, indicating that, in addition to Aβ, an extra N-truncated Aβ fragment was present in the *APPUpp* cell media (Fig. 5G).

To confirm that the reduction of sAPPα in *APPUpp* cell media was α-secretase cleavage specific, we performed Western blot with the same constructs as in the other cell culture–based experiments. When probing with the sAPPα-specific antibody 14D6, sAPPα was found to be reduced ($P < 0.0001$) in *APPUpp* compared to *APPwt* cell media. Moreover, upon treatment with the metalloprotease inhibitor GI254023X that blocks a disintegrin and metalloproteinase 10 (ADAM10), the major α-secretase (*32*) (Fig. 5, H and I), sAPPα was decreased in media from both cell cultures. In addition, and in line with the MSD results (Fig. 5B), sAPPβ was increased ($P < 0.01$) in media from *APPUpp*-transfected cells (Fig. 5, H and I). A mild reduction in total sAPP was observed (Fig. 5, H and I). Moreover, we performed Western blot on the cell lysates using a

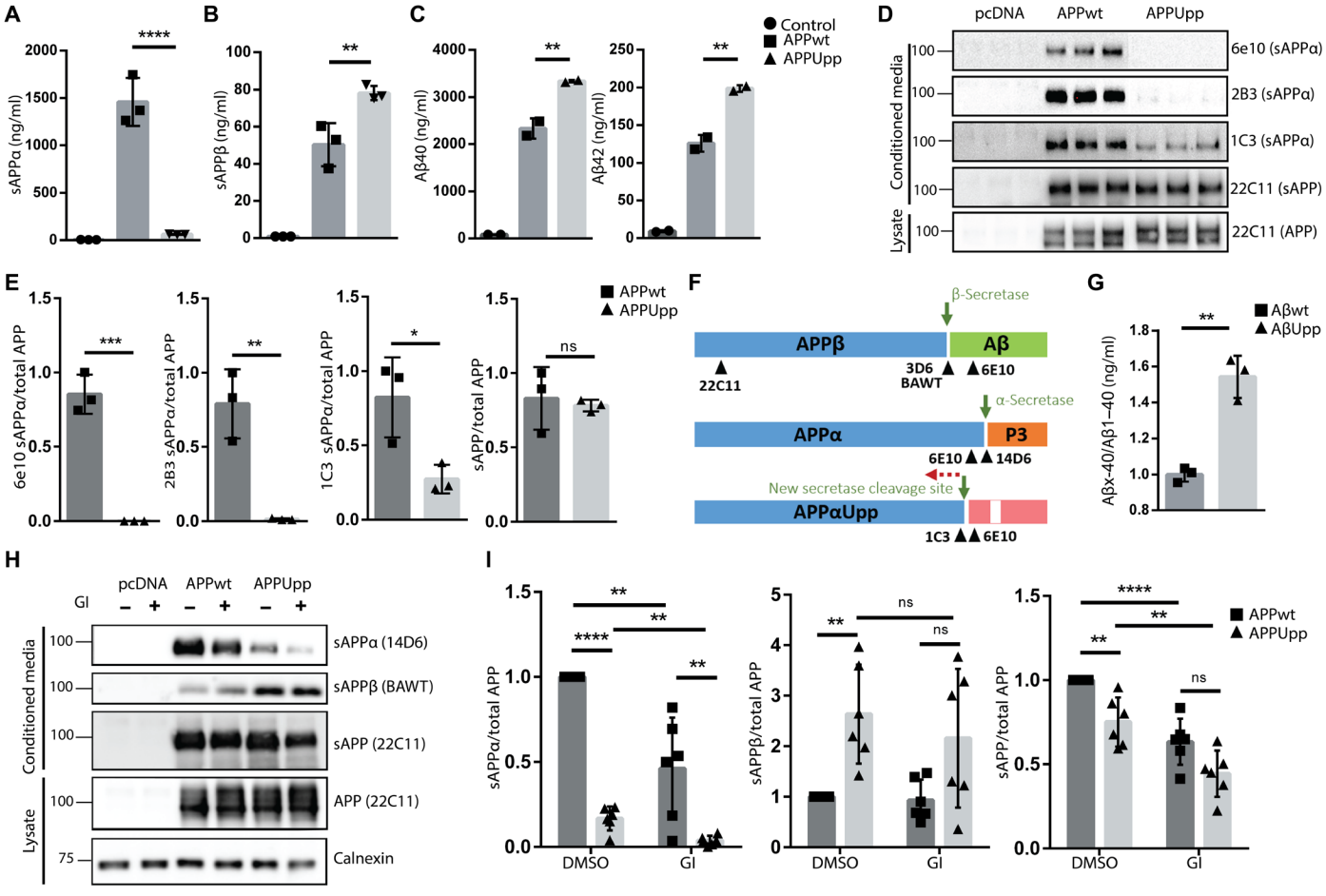

Fig. 5. The *Uppsala APP* mutation alters APP processing. Electrochemiluminescence immunoassay (MSD) analyses of sAPPα (**A**), sAPPβ (**B**), and Aβ40 and Aβ42 (**C**) in conditioned media from HEK293 cells transfected with *APPUpp* as compared to *APPwt* ($n = 3$, $N = 1$). Western blot of *APPUpp* conditioned media, with the sAPPα antibody 2B3 (C terminus), 6E10 (Aβ5–10), and mAb1C3 (Aβ3–8) ($n = 3$, $N = 3$) (**D**). Results from (D) quantified as a ratio of sAPPα (detected with 6E10, 2B3, or 1C3) or total sAPP (detected with 22C11) in cell medium over total APP in cell lysate (**E**). Schematic image indicating β- and α-cleavage sites of APPwt and APPUpp, with antibody binding epitopes indicated (**F**). Ratio of Aβx–40 and Aβ1–40 in *APPwt* and *APPUpp* medium quantified by ELISA ($n = 3$, $N = 3$) (**G**). Western blot analyses of media and lysates from HEK293 cells transiently transfected with *APPwt* or *APPUpp*, with or without the ADAM10-preferring inhibitor GI254023X (GI) using specific antibodies for α- and β-APP ($n = 6$, $N = 4$) (**H**). Results from (H) quantified as a ratio of sAPPα, sAPPβ, or total sAPP in cell medium over total APP in cell lysate (**I**). Statistical significance was determined by one-way ANOVA (A to C) [for (A) and (B), $P < 0.0001$; for (C), Aβ40 and Aβ42, $P = 0.0003$] followed by Tukey's post hoc test, two-tailed unpaired *t* test [$P = 0.004$, 0.0045, 0.0291, and 0.7167 (E) and $P = 0.0016$ (G)], and multiple *t* test (H). All data are represented as group means, and error bars represent SD. *$P < 0.05$, **$P < 0.01$, ***$P < 0.001$, and ****$P < 0.0001$. All results were normalized to total APP. DMSO, dimethyl sulfoxide.

γ-secretase inhibitor [difluorophenylacetyl-alanyl-phenylglycine-t-butyl-ester (DAPT)] to detect C-terminal fragments (CTFs) resulting from α- and β-secretase cleavage of APP and found a slight reduction in CTFα and a more prominent increase in 6E10-postive CTFs (fig. S5).

In addition to the Western blot analyses, we applied MS to investigate the altered APP processing. With respect to *APP*-transfected cells, subjected to IP with 6E10, anti-Aβ40, and anti-Aβ42, the most prominent forms of Aβ were Aβ1–40 and Aβ17–40 in media from *APPwt*-transfected cells (Fig. 6A), whereas AβUpp1–$40_{\Delta 19-24}$ and AβUpp5–$40_{\Delta 19-24}$ were the dominating species in media from *APPUpp*-transfected cells (Fig. 6B), suggesting a new major cleavage of *APPUpp* between amino acids 4 and 5 in the Aβ sequence.

Furthermore, affinity-purified sAPP was digested with the protease LysN, which cleaves proteins at the N-terminal side of lysines, followed by liquid chromatography–tandem MS analyses of peptides that are specific for the cleavage sites of α-secretase and β-secretase. Two different peptides in the N-terminal part of APP, upstream of the α-secretase and β-secretase cleavage sites, respectively, could then be found at similar concentrations in *APPUpp* and *APPwt* cell media (Fig. 6, C and D). Analysis of the α-secretase cleavage site–specific peptide KMDAEFRHDSGYEVHHQK (595–612 in wt hAPP695) showed that cleavage at this site was not significantly reduced ($P = 0.10$) in *APPUpp* compared to *APPWt* media (Fig. 6E). In contrast, the intensity of the β-secretase cleavage site–specific peptide KTEEISEVKM(ox) (587–596 in wt hAPP695) was strongly increased in *APPUpp* in comparison to *APPwt* media ($P < 0.001$), indicating increased cleavage by beta-site APP cleaving enzyme 1 (BACE1), the major β-secretase (Fig. 6F). Moreover, the semi-specific peptide (N terminus specific for LysN, C terminus unspecific) KMDAEFRHDSGY (595–606 in wt hAPP695) was identified. It ends at amino acid 10 of the Aβ sequence (same as the β′-secretase cleavage site) and was found to have a much higher intensity in media from *APPUpp*

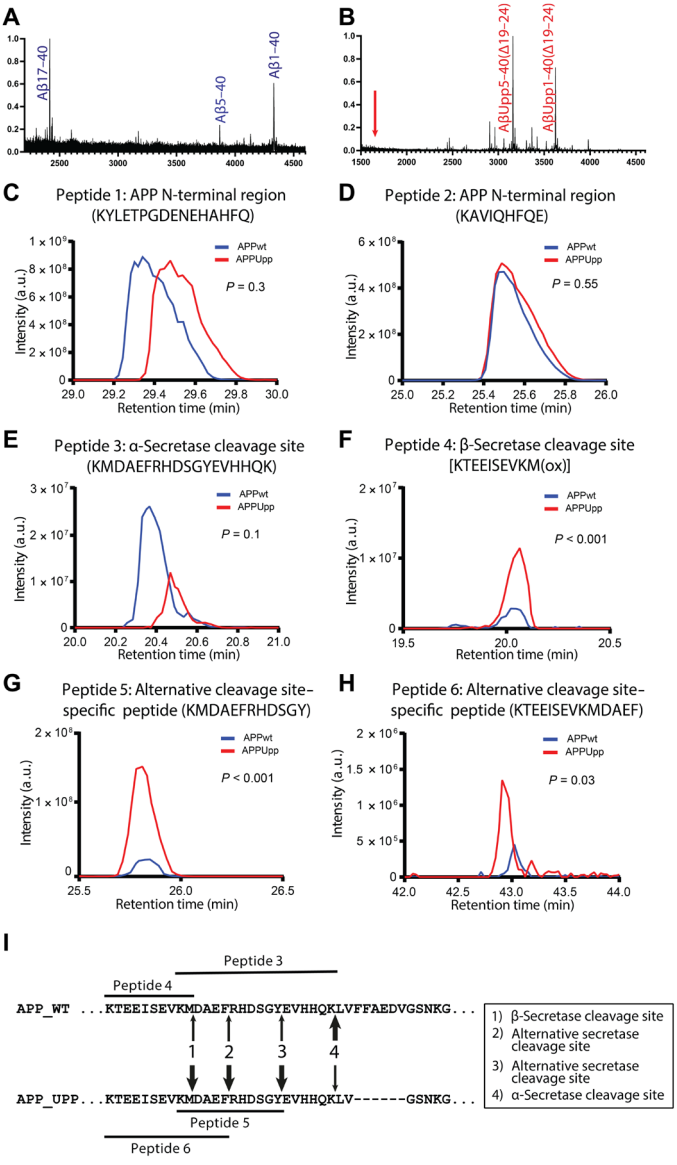

Fig. 6. The *Uppsala APP* mutation increases β-secretase cleavage and alters α-secretase cleavage. MS spectra of the *APPwt*-transfected (**A**) and *APPUpp*-transfected (**B**) HEK293 cells that showed the most prominent peptides present in cell media from cells transfected with either *APPUpp* or *APPwt*. The absence of Upp17–40$_{\Delta 19–24}$ is indicated by the red arrow (B). Extracted ion chromatograms of different peptides of APP (blue, *APPwt*; red, *APPUpp*). Chromatogram of the N-terminal APP peptides, peptide 1, KYLETPGDENEHAHFQ (302–317 in wt hAPP695) (**C**) and peptide 2, KAVIQHFQE (354–362 in wt hAPP695) (**D**). Shifts in retention times between *APPwt* and *APPUpp* were within the normal range of shifts between runs. Chromatogram of the α-secretase cleavage site–specific peptide 3, KMDAEFRHDSGYEVHHQK (595–612 in wt hAPP695, containing one missed LysN cleavage site) (**E**). Chromatogram of the β-cleavage site–specific peptide 4, KTEEISEVKM(ox) (587–596 in wt hAPP695, also containing one missed LysN cleavage site) (**F**). Chromatogram of the semi-specific peptides (N terminus specific for LysN, C terminus unspecific), peptide 5, KMDAEFRHDSGY (595–606 in wt hAPP695) (**G**) and peptide 6, KTEEISEVKMDAEF (587–600 in wt hAPP695) (**H**). (**I**) Cleavage sites of α- and β-secretase are indicated for the sequences of *APPwt* and *APPUpp*. Thick arrows indicate increased and thin arrows indicate decreased cleavage of the two APP sequences.

compared to *APPwt* cells ($P < 0.001$) (Fig. 6G). In addition, a peptide generated upon cleavage between amino acids 4 and 5 of the Aβ sequence, KTEEISEVKMDAEF (587–600 in wt hAPP695), was strongly increased in *APPUpp* media ($P = 0.03$) (Fig. 6H). These MS-based results thus demonstrate activity at two major cleavages sites within the N-terminal part of the Aβ domain of APPUpp. The effects on APP processing revealed by MS analyses are summarized in Fig. 6I. MS sequencing results are shown in fig. S6.

AβUpp1–42$_{\Delta 19–24}$ is prone to form amyloid fibrils in vitro and displays a unique structural polymorphism

To investigate the aggregation behavior of AβUpp, we performed in vitro aggregation experiments. Monomeric Aβ was extracted from solubilized lyophilized synthetic AβUpp1–42$_{\Delta 19–24}$, Aβwt1–42, and AβArc1–42 peptides with high-performance liquid chromatography–size exclusion chromatography (SEC) and analyzed with three different methods upon aggregation at 37°C without shaking.

First, we analyzed fibril formation with the thioflavin T assay (ThT), which revealed that AβUpp1–42$_{\Delta 19–24}$ fibrillizes very rapidly, reaching half of its maximum ThT signal after 0.93 hours, compared to 8.3 hours for Aβwt1–42 and 1.3 hours for AβArc1–42$_{E22G}$. AβUpp1–42$_{\Delta 19–24}$ thus aggregated significantly faster than Aβwt1–42 ($P < 0.0001$) and with a similar rate as AβArc1–42$_{E22G}$, albeit apparently with a somewhat less prominent lag phase (Fig. 7A). The AβUpp1–40$_{\Delta 19–24}$ peptide did not display any fibril formation and was therefore not included in the analysis. Next, we applied an ELISA that selectively measures soluble Aβ oligomers/protofibrils (*33*) and found that the concentration of such Aβ species decreased for AβUpp1–42$_{\Delta 19–24}$, whereas they increased with time for Aβwt1–42 and AβArc1–42 (Fig. 7B). In the same samples (isolated at 1 and 8 hours), the distribution of protofibrillar and monomeric Aβ was qualitatively visualized with SEC. Before SEC analysis, fibrillar Aβ was pelleted with centrifugation, and hence, fibril formation was also indirectly monitored as a decreased size of the protofibril and monomer peaks. Overall, SEC largely confirmed the results from the ThT assay and ELISA, with a prominent decrease of monomeric AβUpp1–42$_{\Delta 19–24}$ over time (from 1 to 8 hours). In addition, similar to the ThT assay and ELISA data and in contrast to Aβwt1–42 and AβArc1–42, no increase in the protofibril peak could be observed over time for AβUpp1–42$_{\Delta 19–24}$ (Fig. 7C).

To further investigate the structural polymorphism of Aβ formed as a result of the *Uppsala APP* mutation, AβUpp1–42$_{\Delta 19–24}$ was fibrillized under a low-pH condition that has previously been shown to yield slow-growing and well-ordered Aβwt1–42 fibrils (*34*). Electron microscopy (EM) imaging of negatively stained fibrils revealed the presence of long and well-ordered fibrils with at least four different polymorphs (Fig. 7D). For higher-resolution examination of these fibrils, cryo-EM experiments were performed. For the two most dominant polymorphs, we obtained three-dimensional density reconstructions at resolutions of 5.7 and 5.1 Å for polymorphs 1 and 2, respectively (Fig. 7D). Both fibrils were found to consist of two symmetric protofilaments. The density allowed for building a tentative backbone trace, but because no side-chain density was visible, the amino acid sequence and also the N- and C-termini could not be assigned to the backbone trace. For both polymorphs, all 36 residues could be accommodated by the density and thus seem to be part of the folded AβUpp1–42$_{\Delta 19–24}$ fibril.

Polymorph 1 (Fig. 7D, middle) resembles an Aβwt1–42 fibril structure that has been earlier described (*35*) and possibly shares the

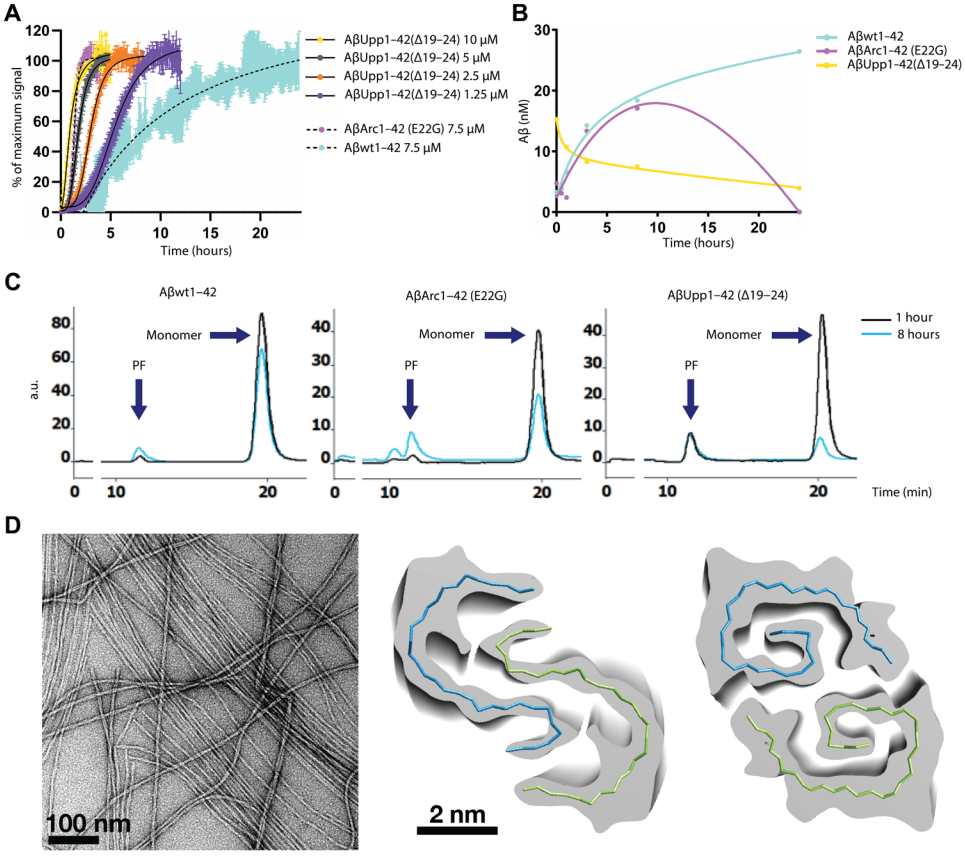

Fig. 7. The *Uppsala APP* mutation accelerates the formation of fibrils. ThT assay of different AβUpp1–42$_{Δ19–24}$, AβArc1–42$_{E22G}$, and Aβwt1–42 (**A**). Concentrations of soluble Aβ oligomers/protofibrils for incubated AβUpp1–42$_{Δ19–24}$, AβArc1–42$_{E22G}$, and Aβwt1–42 samples, as measured by ELISA (**B**) and SEC (**C**). Negative stain EM image of AβUpp1–42$_{Δ19–24}$ fibrils formed at low pH resulted in long, well-ordered fibrils (**D**) (left). Cryo-EM reconstructions (D) (middle and right). For ThT, four replicates of each peptide were aggregating simultaneously ($n = 4$) for each of the three experiments ($N = 3$). Error bars represent SD of the replicates, and black and dashed lines represent curves fitted to the ThT data points. For ELISA, from the same monomeric fraction used for ThT, two replicates ($n = 2$) for each experiment ($N = 3$). SEC was performed one time ($N = 1$). PF, protofibrils.

same protofilament interface in the fibril core (fig. S7). Polymorph 2 has a vague similarity to the previously described Aβwt1–42 structure (*34*), where the prominent salt bridge between the N-terminal Asp[1] and Lys[28] residues could also be present in AβUpp1–42$_{Δ19–24}$ fibrils (fig. S7). However, the C-terminal protofilament interface in the core of the fibril is instead very similar to the interface in two solid-state nuclear magnetic resonance structures of Aβwt1–42 (fig. S8) (*36*, *37*).

DISCUSSION

We here describe the *Uppsala APP* mutation, an *APP* deletion causing a dominantly inherited form of AD. This pathogenic deletion, resulting in a loss of six amino acids in the mid-region of Aβ, was found in three affected family members and not in 500 other subjects, including older nonaffected family members, older healthy controls, and sAD cases.

Most of the AD-causing *APP* mutations lead to symptom onset between 40 and 65 years (*38*), although cases with an even earlier onset have been reported for some mutations (*7*, *9*, *12*). The clinical effects of the *Uppsala APP* mutation are severe, insofar that mutation carriers develop symptoms already in their early forties and have an aggressive disease course. The clinical picture involves severe dementia, characterized by widespread parietotemporal lobe involvement, leading to death from dementia-related illnesses within 5 to 11 years. These clinical characteristics are thus similar to AD in general and to what has been reported for other familial disease variants.

In terms of structural brain imaging, the CT scans displayed the expected symmetrical pattern of global cortical atrophy and mild MTA. As for PET, investigations with the [^{18}F]FDG ligand showed a disease-characteristic hypometabolism of posterior parietal and temporal lobes, whereas analysis with [^{11}C]PIB, which selectively binds to amyloid plaques, only showed a slightly positive pattern. Analyses of postmortem brain tissue from one of the affected cases resulted in several important observations. First, the pathological picture was compatible with AD, including abundant deposition of extracellular Aβ-positive plaques and intracellular tau-positive tangles and neurites accompanied by pronounced gliosis. The regional distribution of Aβ aggregates was extended from neocortex to cerebellum, corresponding to Thal phase 5, and p-tau pathology was observed from locus coeruleus to neocortex, corresponding to Braak stage VI. Second, upon a more detailed examination of tissues from different cortical areas, it became evident that the Aβ pathology of the *Uppsala APP* mutation carriers mainly consists of Aβ42. This observation was corroborated by MALDI-IMS analyses of Aβ plaques from the temporal cortex, which in addition suggested that almost only mutated Aβ was present, either in its full-length version or as N-terminally truncated forms. Third, Aβ plaques were positive for staining with the amyloid dye ThS, which is structurally similar to PIB, raising the question why patients were only slightly [^{11}C]PIB-PET positive, despite high total Aβ concentrations in the postmortem brain tissue analysis. The PET results are displayed as a standard uptake value ratio (SUVR), which is a ratio of the PET signal in the region of interest to the signal from a reference region, in this case the cerebellum. Hence, a low SUVR could have been explained by a high reference region signal, but this interpretation could be ruled out as ThS staining of cerebellum in the patient with *Uppsala APP* revealed a low amyloid burden in this brain region. Although amyloid plaques generally reach the plateau phase rather early in the disease course, we cannot rule out that the time between the scan and the postmortem analyses could explain these differences in patients with *Uppsala APP*. Subtle changes in the fibrillar structure of AβUpp$_{Δ19–24}$ could be another potential explanation for the low PIB retention signal seen for the patients with *Uppsala APP*.

Biochemical analyses of AD CSF biomarkers revealed the expected pathological increase of t-tau and p-tau, whereas, unlike other *APP* mutation cases (*39*), concentrations of Aβ42 were normal for all three *Uppsala APP* mutation carriers investigated. The IP-MS–based CSF analyses suggest an explanation for this unexpected finding, as they demonstrated that the amounts of AβUpp1–$40_{\Delta 19–24}$ and, especially, AβUpp1–$42_{\Delta 19–24}$ produced by the mutated allele were substantially higher than Aβwt1–40 and Aβwt1–42 generated from the nonmutated allele. Thus, an increased generation of Aβ from the allele with the *Uppsala APP* mutation seems to result in higher total CSF concentrations of Aβ1–40 and Aβ1–42 as compared to both sAD cases and controls. Comparison of the IP-MS and routine ELISA-based CSF Aβ data revealed a good correlation for all control and sAD samples, whereas for the *Uppsala APP* mutation carriers, IP-MS–generated CSF Aβ concentrations were relatively higher. The ELISA measurement displayed normal concentrations of Aβ1–42 in CSF from *Uppsala APP* mutation cases, which is higher than in sAD cases, but in the same range as control subjects. We speculate that this discrepancy may be related to a difference in conformation between $AβUpp_{\Delta 19–24}$ and Aβwt. Whereas ELISA detection of Aβ1–42 relies on the simultaneous binding of the assay antibodies to the C and N terminus of Aβ, the IP-MS method is only dependent on one antibody-Aβ interaction at a time, which could facilitate its detection of $AβUpp_{\Delta 19–24}$. We therefore believe that the IP-MS results in this case better reflect the true amounts of Aβ1–42 in CSF, which, in turn, suggests a substantially increased production of Aβ in the brain of *Uppsala APP* mutation carriers.

We next performed cell-based experiments to seek a molecular explanation for the difference in Aβ production from the mutant and wild-type alleles in the mutation carriers. The MSD and Western blot–based analyses of cell media from *APP*-transfected cells, together with analyses of CTF fragments with the 2C11 (C-terminal APP) and 6E10 (Aβ5–10) antibodies on the same cell model, demonstrated an increased production of sAPPβ accompanied by a higher concentration of Aβ in medium from cells transfected with *APPUpp*. The MS analyses of the same cell culture media confirmed an increased β-secretase cleavage, thereby providing an explanation to the elevated amounts of $AβUpp_{\Delta 19–24}$ observed with IP-MS in CSF from the *Uppsala APP* mutation carriers. The detection of an increase in both Aβ and sAPPβ by different methods confirms that the increased CSF $AβUpp_{\Delta 19–24}$ detected by IP-MS was not a method-related artifact.

Because the N-terminal start of the *Uppsala APP* mutation is located only two amino acids from the α-secretase cleavage site, and this enzyme is dependent on the distance from the membrane and not exclusively on a determined cleavage site (*40*–*42*), we reasoned that the mutation may also affect α-secretase activity and/or the location of the cleavage site itself. In line with this, we could demonstrate that α-secretase–related APP processing is indeed altered by the *Uppsala APP* mutation. MSD and Western blot analyses of conditioned media from HEK293 cells transfected with *APPUpp* suggested a strongly decreased α-secretase cleavage at position Aβ16–17. This was further strengthened by analysis of corresponding CTF fragments with the C-terminal APP (2C11) antibody in the same cell model. Moreover, with enzyme inhibition experiments, we could demonstrate that the decreased cleavage indeed was specific to α-secretase. Furthermore, Western blot analysis revealed an additional APP fragment that was faintly detected with mAb1C3 (which binds to Aβ amino acids 3 to 8), but not with 6E10 (which binds to Aβ amino acids 5 to 10) or 2B3 (which binds to an epitope near the C-terminal end of APPα) antibodies, suggesting possible alternative cleavage sites.

To identify the alternative cleavage sites, IP-MS analyses of sAPP fragments secreted in media from *APPUpp*- or *APPwt*-transfected cells were performed and indicated that the mutation results in a new major cleavage site located 12 amino acids N-terminally of the conventional α-secretase cleavage site, between amino acids 4 and 5 of the Aβ sequence. This site was also detected with MS analysis of LysN-digested peptides from media of *APPUpp*-transfected cells. The resulting peptide, AβUpp5–$40_{\Delta 19–24}$, was present in media from *APPUpp* cells to a similar extent as Aβwt17–40 (also known as p3) was in media from *APPwt* cells. Furthermore, AβUpp5–$40_{\Delta 19–24}$ was identified by IP-MS in CSF from *Uppsala APP* mutation carriers, albeit less abundantly than in media from *APPUpp*-transfected HEK293 cells, a cell type that usually has a much higher activity of α-secretase than β-secretase as we could observe with the MSD analyses of the cell culture media. In addition, AβUpp5–$42_{\Delta 19–24}$, likely resulting from the same enzymatic cleavage, was detected by MALDI-IMS in the brain, suggesting that it coaggregates with AβUpp1–$42_{\Delta 19–24}$ into plaques.

Whereas AβUpp5–$40_{\Delta 19–24}$ seems to be consistently present as a result of the *Uppsala APP* mutation, it is at this point unclear whether it is generated as a result of cleavage at an alternative α-secretase site or by some other protease. Several additional proteolytic cleavages of APP may occur within or just outside of the Aβ sequence, for example, by BACE2 or proteases referred to as δ- and η-secretases or by alternative β-secretases, such as meprin-b (*43*–*51*). We speculate, however, that AβUpp5–$40_{\Delta 19–24}$ could be an alternative version of p3 resulting from a shifted α-secretase cleavage, which coaggregates with AβUpp1–$42_{\Delta 19–24}$ to form plaques and thereby contribute to the pathogenesis in mutation carriers. As additional support of its potential pathogenic significance, Aβwt5–42 has, in a previous study, been found to have similar toxicity as Aβwt1–42 but with an even higher propensity to aggregate (*52*). Furthermore, two previous studies have shown that treatment with a BACE1 inhibitor resulted in increased concentrations of Aβ5–40/42 (*53*, *54*), indicating that the cleavage of APPwt between Aβ4 and Aβ5 is indeed independent of β-secretase. Irrespective of the nature of the secretases involved, our data, together with these previous observations, thus suggest that both the β-secretase and the new cleavage site N-terminally of the α-secretase cleavage site are altered by *APPUpp*.

An additional major cleavage site between amino acids 10 and 11 of the Aβ sequence was found to be increased in *APPUpp* compared to *APPwt* cell media. Accordingly, Aβ11–$40_{\Delta 19–24}$ and Aβ11–$42_{\Delta 19–24}$ were identified in CSF from patients with the *Uppsala APP* mutation and in *APPUpp* cell media. Moreover, Aβp11–$42_{\Delta 19–24}$ was abundant in the plaques of the mutation carrier brain, likely as a consequence of increased cleavage at this site. This additional cleavage occurs at the β′ cleavage site, and it is, at this point, uncertain whether the observed activity with the *Uppsala APP* mutation is due to a general increase of BACE1 activity that affects both β-secretase sites in *APPUpp* or whether it represents an additional shifted α-secretase cleavage site resulting from the deletion of six amino acids in the *APPUpp* sequence.

Thus, the *Uppsala APP* mutation seems to abolish the non–amyloid-generating pathway of APP processing, which may further contribute to the pathogenesis in affected individuals. However, to confirm the responsible protease(s) of the additional cleavage sites, further experimental studies using different protease inhibitors are needed.

To investigate the inherent properties of Aβ, we next performed in vitro studies that examined the aggregation behavior of the mutated peptides. Upon analyzing results generated by the ThT assay, it became evident that AβUpp1–42$_{Δ19–24}$ was forming bona fide fibrils very rapidly. With respect to oligomers or protofibrils, both Aβwt1–42 and AβArc1–42 formed such intermediately sized soluble aggregates that increased with time, which is in line with what has been proposed as the pathogenic mechanism for the *Arctic* mutation (*22*). However, AβUpp1–42$_{Δ19–24}$ oligomer/protofibril concentrations decreased over time, probably because the in vitro fibril formation was so rapid and complete that intermediate species were immediately fibrillized. This theory may be supported by the finding that, compared to sAD cases, TBS extracts of the *Uppsala APP* mutation carrier brain displayed lower concentrations of oligomers/protofibrils, especially larger variants, which may suggest that AβUpp$_{Δ19–24}$ aggregates into smaller-sized oligomers that rapidly fibrillize and deposit into plaques. Despite this, oligomers/protofibrils of Aβ are likely to be of relevance for the pathogenesis of AD caused by the *Uppsala APP* mutation.

Structural analyses of two different polymorphs of the *Uppsala APP* mutation revealed that they share some features of previously published Aβ1–42 fibril structures but generally differ from all Aβ fibril structures that have been described to date. Further studies will be required to determine the effects of these structural polymorphs with respect to how they interact with amyloid dyes, such as PIB, and how they may contribute to the formation of toxic Aβ oligomers. Such oligomer formation could be driven by secondary nucleation, which has previously been reported to depend on the structure of the fibrillar surface where such a process is believed to occur (*55*).

To the best of our knowledge, the only previously described intra-Aβ *APP* deletion is the *Osaka* mutation (*30*). Whereas this mutation has been reported to have a recessive character, the *Uppsala APP* mutation is inherited in a dominant manner. Overall, AβUpp1–42$_{Δ19–24}$ seems to be forming amyloid fibrils much more aggressively than the corresponding form of Aβ$_{Osaka}$. For example, an *Osaka APP* mutation knock-in mouse model was reported to display brain pathology only when the inserted gene was homozygously expressed (*56*). In the *Osaka APP* mutation mouse model, a reduced α-secretase cleavage could be observed, similar to what we report here for the *Uppsala APP* mutation (*57*).

Taken together, we have identified an *APP* mutation, which is an intra-Aβ deletion causing dominantly inherited AD. The loss of six amino acids results in an increase of the Aβ promoting β-secretase cleavage, leading to an elevated generation of AβUpp$_{Δ19–24}$ with a concomitant suppression of the regular α-secretase cleavage. Thus, the non–amyloid-generating pathway is seemingly abolished with the mutation. Instead, two other Aβ species, AβUpp5–40/42$_{Δ19–24}$ and AβUpp11–40/42$_{Δ19–24}$, are formed, possibly as a result of a shift of the α-secretase cleavage site, and these may contribute to disease development in mutation carriers. The facts that Aβwt5–42 has previously been reported as pathogenic and that AβUpp5–42$_{Δ19–24}$ was found to be present in plaques from the investigated *Uppsala APP* mutation brain support that, at least, this species may be contributing to the pathogenesis. Moreover, the mutation also renders unique properties to AβUpp1–42$_{Δ19–24}$, which accelerates its fibrillization into distinctive polymorphs and promotes plaque deposition in the affected brains. Thus, the combined effect of three putative pathogenic mechanisms by the *Uppsala APP* mutation may well explain why affected carriers develop an aggressive form of disease with a very early age at symptom onset.

Although the study has clearly identified that the *Uppsala APP* mutation causes AD by a combination of three mechanisms, all related to APP, it is based on a limited patient material from *Uppsala APP* mutation carriers (CSF, $n = 3$ and brain, $n = 1$), which limits the statistical power of certain analyses. Therefore, the exact quantitative impact of the mutation on the development of Aβ and downstream pathologies is difficult to assess, because a certain individual variation between patients is to be expected. Furthermore, although we have identified alterations in APP processing, at both the α- and β-cleavage sites, it remains to be confirmed by which enzymes the cleavages occur. Future studies will also be needed to elucidate the impact of each of the three disease mechanisms presented here, as well as the temporal and structural aspects of the development of Aβ pathology. Some of these future studies could be performed in genetically modified mice carrying the *Uppsala APP* mutation.

MATERIALS AND METHODS

Study design

This study was designed to characterize the clinical and mechanistic features of the herein identified *Uppsala APP* mutation, which results in early onset familial AD. Three members of the "Uppsala family" showing manifest AD symptoms were identified as mutation carriers and subjected to clinical evaluation, structural and amyloid brain imaging, and lumbar puncture for analyses of CSF biomarkers. Furthermore, brain tissue from one of the mutation carriers was analyzed postmortem to assess a range of pathological markers—Aβ, tau, and neuroinflammation—and stage the pathology according to established criteria. Brain tissue was also analyzed with MALDI imaging and immunoassays to investigate the nature of Aβ pathology in comparison with groups of sAD brains ($n = 11$) and neurologically normal control brains ($n = 9$). To study the mechanistic properties of the *Uppsala APP* mutation, MS and immunoassays were used to analyze Aβ and APP fragments resulting from APP processing. Such studies were performed in (i) CSF from the three *Uppsala APP* mutation carriers in comparison with CSF from sAD ($n = 10$) and control ($n = 10$) and (ii) medium and lysate from cell cultures transfected with APP harboring the *Uppsala APP* mutation in comparison with wild-type APP. Last, the aggregation behavior and structure of Aβ aggregates were studied with ThT aggregation assay and cryo-EM. Sample sizes for brain tissue and CSF studies were determined to achieve a statistical power of 80%, based on group differences and variability from previous experience of measurements of Aβ concentrations. Researchers were blinded to sample identity where possible. Selection of the brain tissue and CSF samples is stated in the Supplementary Materials. Figure legends contain the sample sizes, replicate information, and statistical tests used.

Statistics

Statistical analyses were performed using GraphPad Prism (versions 6 and 7). Differences between two groups were evaluated for significance with two-tailed Student's *t* test and multiple *t* test when comparing two treatments. Comparisons of three or more groups on a single dataset were performed by one-way analysis of variance (ANOVA), followed by Tukey's post hoc test. A *P* value threshold of 0.05 was used for the assessment of statistical significance. Values are shown as means ± SD. Individual subject-level data are reported in data files S1 and S2.

SUPPLEMENTARY MATERIALS

stm.sciencemag.org/cgi/content/full/13/606/eabc6184/DC1
Materials and Methods
Figs. S1 to S8
Tables S1 to S3
Data files S1 and S2
References (*58*–*75*)

View/request a protocol for this paper from *Bio-protocol*.

REFERENCES AND NOTES

1. B. T. Hyman, C. H. Phelps, T. G. Beach, E. H. Bigio, N. J. Cairns, M. C. Carrillo, D. W. Dickson, C. Duyckaerts, M. P. Frosch, E. Masliah, S. S. Mirra, P. T. Nelson, J. A. Schneider, D. R. Thal, B. Thies, J. Q. Trojanowski, H. V. Vinters, T. J. Montine, National Institute on Aging-Alzheimer's Association guidelines for the neuropathologic assessment of Alzheimer's disease. *Alzheimers Dement.* **8**, 1–13 (2012).
2. D. J. Selkoe, J. Hardy, The amyloid hypothesis of Alzheimer's disease at 25 years. *EMBO Mol. Med.* **8**, 595–608 (2016).
3. A. Goate, M. C. Chartier-Harlin, M. Mullan, J. Brown, F. Crawford, L. Fidani, L. Giuffra, A. Haynes, N. Irving, L. James, R. Mant, P. Newton, K. Rooke, P. Roques, C. Talbot, M. Pericak-Vance, A. Roses, R. Williamson, M. Rossor, M. Owen, J. Hardy, Segregation of a missense mutation in the amyloid precursor protein gene with familial Alzheimer's disease. *Nature* **349**, 704–706 (1991).
4. J. Murrell, M. Farlow, B. Ghetti, M. D. Benson, A mutation in the amyloid precursor protein associated with hereditary Alzheimer's disease. *Science* **254**, 97–99 (1991).
5. M.-C. Chartier-Harlin, F. Crawfort, H. Houlden, A. Warren, D. Hughes, L. Fidani, A. Goate, M. Rossor, P. Roques, J. Hardy, M. Mullan, Early-onset Alzheimer's disease caused by mutations at codon 717 of the β-amyloid precursor protein gene. *Nature* **353**, 844–846 (1991).
6. C. Eckman, N. Mehta, R. Crook, J. Perez-Tur, G. Prihar, E. Pfeiffer, N. Graff-Radford, P. Hinder, D. Yager, B. Zenk, L. Refolo, C. Prada, S. Younkin, M. Hutton, J. Hardy, A new pathogenic mutation in the APP gene (I716V) increases the relative proportion of Aβ42(43). *Hum. Mol. Genet.* **6**, 2087–2089 (1997).
7. J. R. Murrell, A. M. Hake, K. A. Quaid, M. R. Farlow, B. Ghetti, Early-onset Alzheimer disease caused by a new mutation (V717L) in the amyloid precursor protein gene. *Arch. Neurol.* **57**, 885–887 (2000).
8. J. B. Kwok, Q. X. Li, M. Hallupp, S. Whyte, D. Ames, K. Beyreuther, C. L. Masters, P. R. Schofield, Novel Leu723Pro amyloid precursor protein mutation increases amyloid β42(43) peptide levels and induces apoptosis. *Ann. Neurol.* **47**, 249–253 (2000).
9. S. Kumar-Singh, C. De Jonghe, M. Cruts, R. Kleinert, R. Wang, M. Mercken, B. De Strooper, H. Vanderstichele, A. Löfgren, I. Vanderhoeven, H. Backhovens, E. Vanmechelen, P. Kroisel, C. Van Broeckhoven, Nonfibrillar diffuse amyloid deposition due to a γ_{42}-secretase site mutation points to an essential role for N-truncated $A\beta_{42}$ in Alzheimer's disease. *Hum. Mol. Genet.* **9**, 2589–2598 (2000).
10. M. Cruts, B. Dermaut, R. Rademakers, M. Van den Broeck, F. Stögbauer, C. Van Broeckhoven, Novel APP mutation V715A associated with presenile Alzheimer's disease in a German family. *J. Neurol.* **250**, 1374–1375 (2003).
11. J. Theuns, E. Marjaux, M. Vandenbulcke, K. Van Laere, S. Kumar-Singh, G. Bormans, N. Brouwers, M. Van den Broeck, K. Vennekens, E. Corsmit, M. Cruts, B. De Strooper, C. Van Broeckhoven, R. Vandenberghe, Alzheimer dementia caused by a novel mutation located in the APP C-terminal intracytosolic fragment. *Hum. Mutat.* **27**, 888–896 (2006).
12. R. J. Guerreiro, M. Baquero, R. Blesa, M. Boada, J. M. Bras, M. J. Bullido, A. Calado, R. Crook, C. Ferreira, A. Frank, T. Gomez-Isla, I. Hernandez, A. Lleo, A. Machado, P. Martinez-Lage, J. Masdeu, L. Molina-Porcel, J. L. Molinuevo, P. Pastor, J. Perez-Tur, R. Relvas, C. R. Oliveira, M. H. Ribeiro, E. Rogaeva, A. Sa, L. Samaranch, R. Sanchez-Valle, I. Santana, L. Tarraga, F. Valdivieso, A. Singleton, J. Hardy, J. Clarimon, Genetic screening of Alzheimer's disease genes in Iberian and African samples yields novel mutations in presenilins and APP. *Neurobiol. Aging* **31**, 725–731 (2010).
13. Q. Wang, J. Jia, W. Qin, L. Wu, D. Li, Q. Wang, H. Li, A novel AβPP M722K mutation affects amyloid-β secretion and tau phosphorylation and may cause early-onset familial Alzheimer's disease in Chinese individuals. *J. Alzheimers Dis.* **47**, 157–165 (2015).
14. S. Hsu, B. A. Gordon, R. Hornbeck, J. B. Norton, D. Levitch, A. Louden, E. Ziegemeier, R. Laforce Jr., J. Chhatwal, G. S. Day, E. McDade, J. C. Morris, A. M. Fagan, T. L. S. Benzinger, A. M. Goate, C. Cruchaga, R. J. Bateman; Dominantly Inherited Alzheimer Network (DIAN), C. M. Karch, Discovery and validation of autosomal dominant Alzheimer's disease mutations. *Alzheimers Res. Ther.* **10**, 67 (2018).
15. M. Citron, C. Vigo-Pelfrey, D. B. Teplow, C. Miller, D. Schenk, J. Johnston, B. Winblad, N. Venizelos, L. Lannfelt, D. J. Selkoe, Excessive production of amyloid beta-protein by peripheral cells of symptomatic and presymptomatic patients carrying the Swedish familial Alzheimer disease mutation. *Proc. Natl. Acad. Sci. U.S.A.* **91**, 11993–11997 (1994).
16. J. A. Johnston, R. F. Cowburn, S. Norgren, B. Wiehager, N. Venizelos, B. Winblad, C. Vigo-Pelfrey, D. Schenk, L. Lannfelt, C. O'Neill, Increased β-amyloid release and levels of amyloid precursor protein (APP) in fibroblast cell lines from family members with the Swedish Alzheimer's disease APP670/671 mutation. *FEBS Lett.* **354**, 274–278 (1994).
17. D. Scheuner, C. Eckman, M. Jensen, X. Song, M. Citron, N. Suzuki, T. D. Bird, J. Hardy, M. Hutton, W. Kukull, E. Larson, E. Levy-Lahad, M. Viitanen, E. Peskind, P. Poorkaj, G. Schellenberg, R. Tanzi, W. Wasco, L. Lannfelt, D. Selkoe, S. Younkin, Secreted amyloid β–protein similar to that in the senile plaques of Alzheimer's disease is increased in vivo by the presenilin 1 and 2 and *APP* mutations linked to familial Alzheimer's disease. *Nat. Med.* **2**, 864–870 (1996).
18. E. Levy, M. D. Carman, I. J. Fernandez-Madrid, M. D. Power, I. Lieberburg, S. G. van Duinen, G. T. Bots, W. Luyendijk, B. Frangione, Mutation of the Alzheimer's disease amyloid gene in hereditary cerebral hemorrhage, Dutch type. *Science* **248**, 1124–1126 (1990).
19. O. Bugiani, G. Giaccone, G. Rossi, M. Mangieri, R. Capobianco, M. Morbin, G. Mazzoleni, C. Cupidi, G. Marcon, A. Giovagnoli, A. Bizzi, G. Di Fede, G. Puoti, F. Carella, A. Salmaggi, A. Romorini, G. M. Patruno, M. Magoni, A. Padovani, F. Tagliavini, Hereditary cerebral hemorrhage with amyloidosis associated with the E693K mutation of APP. *Arch. Neurol.* **67**, 987–995 (2010).
20. L. Hendriks, C. M. van Duijn, P. Cras, M. Cruts, W. Van Hul, F. Van Harskamp, A. Warren, M. G. McInnis, S. E. Antonarakis, J.-J. Martin, A. Hofman, C. Van Broeckhoven, Presenile dementia and cerebral haemorrhage linked to a mutation at codon 692 of the β–amyloid precursor protein gene. *Nat. Genet.* **1**, 218–221 (1992).
21. T. J. Grabowski, H. S. Cho, J. P. Vonsattel, G. W. Rebeck, S. M. Greenberg, Novel amyloid precursor protein mutation in an Iowa family with dementia and severe cerebral amyloid angiopathy. *Ann. Neurol.* **49**, 697–705 (2001).
22. C. Nilsberth, A. Westlind-Danielsson, C. B. Eckman, M. M. Condron, K. Axelman, C. Forsell, C. Stenh, J. Luthman, D. B. Teplow, S. G. Younkin, J. Näslund, L. Lannfelt, The 'Arctic' APP mutation (E693G) causes Alzheimer's disease by enhanced Aβ protofibril formation. *Nat. Neurosci.* **4**, 887–893 (2001).
23. A.-S. Johansson, F. Berglind-Dehlin, G. Karlsson, K. Edwards, P. Gellerfors, L. Lannfelt, Physiochemical characterization of the Alzheimer's disease-related peptides Aβ1–42Arctic and Aβ1–42wt. *FEBS J.* **273**, 2618–2630 (2006).
24. H. Basun, N. Bogdanovic, M. Ingelsson, O. Almkvist, J. Naslund, K. Axelman, T. D. Bird, D. Nochlin, G. D. Schellenberg, L. O. Wahlund, L. Lannfelt, Clinical and neuropathological features of the arctic APP gene mutation causing early-onset Alzheimer disease. *Arch. Neurol.* **65**, 499–505 (2008).
25. O. Philipson, A. Lord, M. Lalowski, R. Soliymani, M. Baumann, J. Thyberg, N. Bogdanovic, T. Olofsson, L. O. Tjernberg, M. Ingelsson, L. Lannfelt, H. Kalimo, L. N. Nilsson, The Arctic amyloid-β precursor protein (AβPP) mutation results in distinct plaques and accumulation of N- and C-truncated Aβ. *Neurobiol. Aging* **33**, 1010.e1–1010.e1011013 (2012).
26. H. Kalimo, M. Lalowski, N. Bogdanovic, O. Philipson, T. D. Bird, D. Nochlin, G. D. Schellenberg, R. Brundin, T. Olofsson, R. Soliymani, M. Baumann, O. Wirths, T. A. Bayer, L. N. Nilsson, H. Basun, L. Lannfelt, M. Ingelsson, The Arctic AβPP mutation leads to Alzheimer's disease pathology with highly variable topographic deposition of differentially truncated Aβ. *Acta Neuropathol. Commun.* **1**, 60 (2013).
27. T. Jonsson, J. K. Atwal, S. Steinberg, J. Snaedal, P. V. Jonsson, S. Bjornsson, H. Stefansson, P. Sulem, D. Gudbjartsson, J. Maloney, K. Hoyte, A. Gustafson, Y. Liu, Y. Lu, T. Bhangale, R. R. Graham, J. Huttenlocher, G. Bjornsdottir, O. A. Andreassen, E. G. Jonsson, A. Palotie, T. W. Behrens, O. T. Magnusson, A. Kong, U. Thorsteinsdottir, R. J. Watts, K. Stefansson, A mutation in APP protects against Alzheimer's disease and age-related cognitive decline. *Nature* **488**, 96–99 (2012).
28. J. A. Maloney, T. Bainbridge, A. Gustafson, S. Zhang, R. Kyauk, P. Steiner, M. van der Brug, Y. Liu, J. A. Ernst, R. J. Watts, J. K. Atwal, Molecular mechanisms of Alzheimer disease protection by the A673T allele of amyloid precursor protein. *J. Biol. Chem.* **289**, 30990–31000 (2014).
29. I. Benilova, R. Gallardo, A. A. Ungureanu, V. Castillo Cano, A. Snellinx, M. Ramakers, C. Bartic, F. Rousseau, J. Schymkowitz, B. De Strooper, The Alzheimer disease protective mutation A2T modulates kinetic and thermodynamic properties of amyloid-β (Aβ) aggregation. *J. Biol. Chem.* **289**, 30977–30989 (2014).
30. K. Nishitsuji, T. Tomiyama, K. Ishibashi, K. Ito, R. Teraoka, M. P. Lambert, W. L. Klein, H. Mori, The E693Delta mutation in amyloid precursor protein increases intracellular accumulation of amyloid beta oligomers and causes endoplasmic reticulum stress-induced apoptosis in cultured cells. *Am. J. Pathol.* **174**, 957–969 (2009).
31. S. Abu Hamdeh, E. R. Waara, C. Moller, L. Soderberg, H. Basun, I. Alafuzoff, L. Hillered, L. Lannfelt, M. Ingelsson, N. Marklund, Rapid amyloid-β oligomer and protofibril accumulation in traumatic brain injury. *Brain Pathol.* **28**, 451–462 (2018).
32. P. H. Kuhn, H. Wang, B. Dislich, A. Colombo, U. Zeitschel, J. W. Ellwart, E. Kremmer, S. Rossner, S. F. Lichtenthaler, ADAM10 is the physiologically relevant, constitutive alpha-secretase of the amyloid precursor protein in primary neurons. *EMBO J.* **29**, 3020–3032 (2010).

33. H. Englund, D. Sehlin, A. S. Johansson, L. N. Nilsson, P. Gellerfors, S. Paulie, L. Lannfelt, F. E. Pettersson, Sensitive ELISA detection of amyloid-beta protofibrils in biological samples. *J. Neurochem.* **103**, 334–345 (2007).
34. L. Gremer, D. Schölzel, C. Schenk, E. Reinartz, J. Labahn, R. B. G. Ravelli, M. Tusche, C. Lopez-Iglesias, W. Hoyer, H. Heise, D. Willbold, G. F. Schröder, Fibril structure of amyloid-β(1–42) by cryo–electron microscopy. *Science* **358**, 116–119 (2017).
35. M. Schmidt, A. Rohou, K. Lasker, J. K. Yadav, C. Schiene-Fischer, M. Fandrich, N. Grigorieff, Peptide dimer structure in an Aβ(1–42) fibril visualized with cryo-EM. *Proc. Natl. Acad. Sci. U.S.A.* **112**, 11858–11863 (2015).
36. M. T. Colvin, R. Silvers, Q. Z. Ni, T. V. Can, I. Sergeyev, M. Rosay, K. J. Donovan, B. Michael, J. Wall, S. Linse, R. G. Griffin, Atomic resolution structure of monomorphic Aβ42 amyloid fibrils. *J. Am. Chem. Soc.* **138**, 9663–9674 (2016).
37. M. A. Walti, F. Ravotti, H. Arai, C. G. Glabe, J. S. Wall, A. Bockmann, P. Guntert, B. H. Meier, R. Riek, Atomic-resolution structure of a disease-relevant Aβ(1–42) amyloid fibril. *Proc. Natl. Acad. Sci. U.S.A.* **113**, E4976–E4984 (2016).
38. N. S. Ryan, M. N. Rossor, Correlating familial Alzheimer's disease gene mutations with clinical phenotype. *Biomark. Med.* **4**, 99–112 (2010).
39. R. J. Bateman, C. Xiong, T. L. Benzinger, A. M. Fagan, A. Goate, N. C. Fox, D. S. Marcus, N. J. Cairns, X. Xie, T. M. Blazey, D. M. Holtzman, A. Santacruz, V. Buckles, A. Oliver, K. Moulder, P. S. Aisen, B. Ghetti, W. E. Klunk, E. McDade, R. N. Martins, C. L. Masters, R. Mayeux, J. M. Ringman, M. N. Rossor, P. R. Schofield, R. A. Sperling, S. Salloway, J. C. Morris; Dominantly Inherited Alzheimer Network, Clinical and biomarker changes in dominantly inherited Alzheimer's disease. *N. Engl. J. Med.* **367**, 795–804 (2012).
40. S. S. Sisodia, Beta-amyloid precursor protein cleavage by a membrane-bound protease. *Proc. Natl. Acad. Sci. U.S.A.* **89**, 6075–6079 (1992).
41. P. Saftig, S. F. Lichtenthaler, The alpha secretase ADAM10: A metalloprotease with multiple functions in the brain. *Prog. Neurobiol.* **135**, 1–20 (2015).
42. S. F. Lichtenthaler, M. K. Lemberg, R. Fluhrer, Proteolytic ectodomain shedding of membrane proteins in mammals-hardware, concepts, and recent developments. *EMBO J.* **37**, e99456 (2018).
43. M. Farzan, C. E. Schnitzler, N. Vasilieva, D. Leung, H. Choe, BACE2, a beta -secretase homolog, cleaves at the beta site and within the amyloid-beta region of the amyloid-beta precursor protein. *Proc. Natl. Acad. Sci. U.S.A.* **97**, 9712–9717 (2000).
44. E. Portelius, G. Brinkmalm, A. J. Tran, H. Zetterberg, A. Westman-Brinkmalm, K. Blennow, Identification of novel APP/Abeta isoforms in human cerebrospinal fluid. *Neurodegener Dis* **6**, 87–94 (2009).
45. J. Bien, T. Jefferson, M. Causevic, T. Jumpertz, L. Munter, G. Multhaup, S. Weggen, C. Becker-Pauly, C. U. Pietrzik, The metalloprotease meprin β generates amino terminal-truncated amyloid β peptide species. *J. Biol. Chem.* **287**, 33304–33313 (2012).
46. E. Portelius, M. Olsson, G. Brinkmalm, U. Rüetschi, N. Mattsson, U. Andreasson, J. Gobom, A. Brinkmalm, M. Hölttä, K. Blennow, H. Zetterberg, Mass spectrometric characterization of amyloid-β species in the 7PA2 cell model of Alzheimer's disease. *J. Alzheimers Dis.* **33**, 85–93 (2013).
47. A. T. Welzel, J. E. Maggio, G. M. Shankar, D. E. Walker, B. L. Ostaszewski, S. Li, I. Klyubin, M. J. Rowan, P. Seubert, D. M. Walsh, D. J. Selkoe, Secreted amyloid β-proteins in a cell culture model include N-terminally extended peptides that impair synaptic plasticity. *Biochemistry* **53**, 3908–3921 (2014).
48. N. Kaneko, R. Yamamoto, T. A. Sato, K. Tanaka, Identification and quantification of amyloid beta-related peptides in human plasma using matrix-assisted laser desorption/ionization time-of-flight mass spectrometry. *Proc. Jpn. Acad. Ser. B Phys. Biol. Sci.* **90**, 104–117 (2014).
49. M. Willem, S. Tahirovic, M. A. Busche, S. V. Ovsepian, M. Chafai, S. Kootar, D. Hornburg, L. D. Evans, S. Moore, A. Daria, H. Hampel, V. Muller, C. Giudici, B. Nuscher, A. Wenninger-Weinzierl, E. Kremmer, M. T. Heneka, D. R. Thal, V. Giedraitis, L. Lannfelt, U. Müller, F. J. Livesey, F. Meissner, J. Herms, A. Konnerth, H. Marie, C. Haass, η-Secretase processing of APP inhibits neuronal activity in the hippocampus. *Nature* **526**, 443–447 (2015).
50. Z. Zhang, M. Song, X. Liu, S. S. Kang, D. M. Duong, N. T. Seyfried, X. Cao, L. Cheng, Y. E. Sun, S. Ping Yu, J. Jia, A. I. Levey, K. Ye, Delta-secretase cleaves amyloid precursor protein and regulates the pathogenesis in Alzheimer's disease. *Nat. Commun.* **6**, 8762 (2015).
51. K. Baranger, Y. Marchalant, A. E. Bonnet, N. Crouzin, A. Carrete, J. M. Paumier, N. A. Py, A. Bernard, C. Bauer, E. Charrat, K. Moschke, M. Seiki, M. Vignes, S. F. Lichtenthaler, F. Checler, M. Khrestchatisky, S. Rivera, MT5-MMP is a new pro-amyloidogenic proteinase that promotes amyloid pathology and cognitive decline in a transgenic mouse model of Alzheimer's disease. *Cell. Mol. Life Sci.* **73**, 217–236 (2016).
52. T. Weiffert, G. Meisl, P. Flagmeier, S. De, C. J. R. Dunning, B. Frohm, H. Zetterberg, K. Blennow, E. Portelius, D. Klenerman, C. M. Dobson, T. P. J. Knowles, S. Linse, Increased secondary nucleation underlies accelerated aggregation of the four-residue N-terminally truncated Aβ42 species Aβ5–42. *ACS Chem. Neurosci.* **10**, 2374–2384 (2019).
53. N. Mattsson, L. Rajendran, H. Zetterberg, M. Gustavsson, U. Andreasson, M. Olsson, G. Brinkmalm, J. Lundkvist, L. H. Jacobson, L. Perrot, U. Neumann, H. Borghys, M. Mercken, D. Dhuyvetter, F. Jeppsson, K. Blennow, E. Portelius, BACE1 inhibition induces a specific cerebrospinal fluid β-amyloid pattern that identifies drug effects in the central nervous system. *PLOS ONE* **7**, e31084 (2012).
54. E. Portelius, R. A. Dean, U. Andreasson, N. Mattsson, A. Westerlund, M. Olsson, R. B. Demattos, M. M. Racke, H. Zetterberg, P. C. May, K. Blennow, β-site amyloid precursor protein-cleaving enzyme 1(BACE1) inhibitor treatment induces Aβ5-X peptides through alternative amyloid precursor protein cleavage. *Alzheimers Res. Ther.* **6**, 75 (2014).
55. S. Linse, Monomer-dependent secondary nucleation in amyloid formation. *Biophys. Rev.* **9**, 329–338 (2017).
56. T. Umeda, T. Kimura, K. Yoshida, K. Takao, Y. Fujita, S. Matsuyama, A. Sakai, M. Yamashita, Y. Yamashita, K. Ohnishi, M. Suzuki, H. Takuma, T. Miyakawa, A. Takashima, T. Morita, H. Mori, T. Tomiyama, Mutation-induced loss of APP function causes GABAergic depletion in recessive familial Alzheimer's disease: Analysis of Osaka mutation-knockin mice. *Acta Neuropathol. Commun.* **5**, 59 (2017).
57. L. Kulic, J. McAfoose, T. Welt, C. Tackenberg, C. Spani, F. Wirth, V. Finder, U. Konietzko, M. Giese, A. Eckert, K. Noriaki, T. Shimizu, K. Murakami, K. Irie, S. Rasool, C. Glabe, C. Hock, R. M. Nitsch, Early accumulation of intracellular fibrillar oligomers and late congophilic amyloid angiopathy in mice expressing the Osaka intra-Aβ APP mutation. *Transl. Psychiatry* **2**, e183 (2012).
58. G. McKhann, D. Drachman, M. Folstein, R. Katzman, D. Price, E. M. Stadlan, Clinical diagnosis of Alzheimer's disease: Report of the NINCDS-ADRDA Work Group under the auspices of department of health and human services task force on Alzheimer's disease. *Neurology* **34**, 939–944 (1984).
59. C. E. Teunissen, A. Petzold, J. L. Bennett, F. S. Berven, L. Brundin, M. Comabella, D. Franciotta, J. L. Frederiksen, J. O. Fleming, R. Furlan, R. Q. Hintzen, S. G. Hughes, M. H. Johnson, E. Krasulova, J. Kuhle, M. C. Magnone, C. Rajda, K. Rejdak, H. K. Schmidt, V. van Pesch, E. Waubant, C. Wolf, G. Giovannoni, B. Hemmer, H. Tumani, F. Deisenhammer, A consensus protocol for the standardization of cerebrospinal fluid collection and biobanking. *Neurology* **73**, 1914–1922 (2009).
60. A. Elobeid, S. Libard, M. Leino, S. N. Popova, I. Alafuzoff, Altered proteins in the aging brain. *J. Neuropathol. Exp. Neurol.* **75**, 316–325 (2016).
61. O. Philipson, P. Hammarström, K. P. Nilsson, E. Portelius, T. Olofsson, M. Ingelsson, B. T. Hyman, K. Blennow, L. Lannfelt, H. Kalimo, L. N. Nilsson, A highly insoluble state of Abeta similar to that of Alzheimer's disease brain is found in Arctic APP transgenic mice. *Neurobiol. Aging* **30**, 1393–1405 (2009).
62. W. Michno, S. Nystrom, P. Wehrli, T. Lashley, G. Brinkmalm, L. Guerard, S. Syvanen, D. Sehlin, I. Kaya, D. Brinet, K. P. R. Nilsson, P. Hammarstrom, K. Blennow, H. Zetterberg, J. Hanrieder, Pyroglutamation of amyloid-βx-42 (Aβx-42) followed by Aβ1–40 deposition underlies plaque polymorphism in progressing Alzheimer's disease pathology. *J. Biol. Chem.* **294**, 6719–6732 (2019).
63. T. Klingstedt, A. Aslund, R. A. Simon, L. B. Johansson, J. J. Mason, S. Nyström, P. Hammarström, K. P. Nilsson, Synthesis of a library of oligothiophenes and their utilization as fluorescent ligands for spectral assignment of protein aggregates. *Org. Biomol. Chem.* **9**, 8356–8370 (2011).
64. J. Rasmussen, J. Mahler, N. Beschorner, S. A. Kaeser, L. M. Hasler, F. Baumann, S. Nystrom, E. Portelius, K. Blennow, T. Lashley, N. C. Fox, D. Sepulveda-Falla, M. Glatzel, A. L. Oblak, B. Ghetti, K. P. R. Nilsson, P. Hammarstrom, M. Staufenbiel, L. C. Walker, M. Jucker, Amyloid polymorphisms constitute distinct clouds of conformational variants in different etiological subtypes of Alzheimer's disease. *Proc. Natl. Acad. Sci. U.S.A.* **114**, 13018–13023 (2017).
65. E. Portelius, A. Westman-Brinkmalm, H. Zetterberg, K. Blennow, Determination of beta-amyloid peptide signatures in cerebrospinal fluid using immunoprecipitation-mass spectrometry. *J. Proteome Res.* **5**, 1010–1016 (2006).
66. E. Portelius, A. J. Tran, U. Andreasson, R. Persson, G. Brinkmalm, H. Zetterberg, K. Blennow, A. Westman-Brinkmalm, Characterization of amyloid beta peptides in cerebrospinal fluid by an automated immunoprecipitation procedure followed by mass spectrometry. *J. Proteome Res.* **6**, 4433–4439 (2007).
67. G. Brinkmalm, E. Portelius, A. Ohrfelt, N. Mattsson, R. Persson, M. K. Gustavsson, C. H. Vite, J. Gobom, J. E. Mansson, J. Nilsson, A. Halim, G. Larson, U. Ruetschi, H. Zetterberg, K. Blennow, A. Brinkmalm, An online nano-LC-ESI-FTICR-MS method for comprehensive characterization of endogenous fragments from amyloid β and amyloid precursor protein in human and cat cerebrospinal fluid. *J. Mass Spectrom.* **47**, 591–603 (2012).
68. A. Ludwig, C. Hundhausen, M. H. Lambert, N. Broadway, R. C. Andrews, D. M. Bickett, M. A. Leesnitzer, J. D. Becherer, Metalloproteinase inhibitors for the disintegrin-like metalloproteinases ADAM10 and ADAM17 that differentially block constitutive and phorbol ester-inducible shedding of cell surface molecules. *Comb. Chem. High Throughput Screen.* **8**, 161–171 (2005).
69. A. Colombo, H. Wang, P. H. Kuhn, R. Page, E. Kremmer, P. J. Dempsey, H. C. Crawford, S. F. Lichtenthaler, Constitutive α- and β-secretase cleavages of the amyloid precursor protein are partially coupled in neurons, but not in frequently used cell lines. *Neurobiol. Dis.* **49**, 137–147 (2013).

70. P. H. Kuhn, K. Koroniak, S. Hogl, A. Colombo, U. Zeitschel, M. Willem, C. Volbracht, U. Schepers, A. Imhof, A. Hoffmeister, C. Haass, S. Rossner, S. Brase, S. F. Lichtenthaler, Secretome protein enrichment identifies physiological BACE1 protease substrates in neurons. *EMBO J.* **31**, 3157–3168 (2012).
71. C. Höfling, M. Morawski, U. Zeitschel, E. R. Zanier, K. Moschke, A. Serdaroglu, F. Canneva, S. von Horsten, M. G. De Simoni, G. Forloni, C. Jäger, E. Kremmer, S. Roßner, S. F. Lichtenthaler, P.-H. Kuhn, Differential transgene expression patterns in Alzheimer mouse models revealed by novel human amyloid precursor protein-specific antibodies. *Aging Cell* **15**, 953–963 (2016).
72. C. S. Hughes, S. Foehr, D. A. Garfield, E. E. Furlong, L. M. Steinmetz, J. Krijgsveld, Ultrasensitive proteome analysis using paramagnetic bead technology. *Mol. Syst. Biol.* **10**, 757 (2014).
73. J. Cox, M. Y. Hein, C. A. Luber, I. Paron, N. Nagaraj, M. Mann, Accurate proteome-wide label-free quantification by delayed normalization and maximal peptide ratio extraction, termed MaxLFQ. *Mol. Cell. Proteomics* **13**, 2513–2526 (2014).
74. J. Zivanov, T. Nakane, B. O. Forsberg, D. Kimanius, W. J. Hagen, E. Lindahl, S. H. Scheres, New tools for automated high-resolution cryo-EM structure determination in RELION-3. *eLife* **7**, e42166 (2018).
75. A. Rohou, N. Grigorieff, CTFFIND4: Fast and accurate defocus estimation from electron micrographs. *J. Struct. Biol.* **192**, 216–221 (2015).

Acknowledgments: We thank C. Röder and L. Gremer for help with sample preparation for cryo-EM, discussions, and advice. We also thank P. Hammarström and P. Nilsson for providing fluorophores q-FTAA and h-FTAA. We also thank the Uppsala Genome Center for the help with targeted exome sequencing, L. Streubel-Gallasch for statistical advice, H. Zetterberg for assistance with CSF ELISA measurements, and J. Watts for critical proofreading of the manuscript. Last, Fig. 1G was made in part using Biorender. **Funding:** This work was supported by the Swedish Research Council (#2016-02120 to L.L. and #2018-02181 to J.H.); the Swedish Alzheimer Foundation (to L.L. and J.H.); the Swedish Brain Foundation (to L.L.); Åke Wibergs Stiftelse (to J.H.); Åhlén Stiftelsen (to J.H.); the German Research Foundation within the framework of the Munich Cluster for Systems Neurology (EXC 2145 SyNergy, project ID 390857198) and the research unit FOR2290, the BMBF within project CLINSPECT-M, and by JPco-fuND2 2019 Personalized Medicine for Neurodegenerative Diseases 01ED2002B (to S.F.L.). **Author contributions:** M.P.d.l.V., V.G., L.L., D.S., and M.I. designed the study. L.L. obtained the funding. These authors performed the experiments: M.P.d.l.V. (genetic analyses, immunostainings, ELISAs, ThS staining, cell transfection, Western blot, Meso Scale electrochemiluminescence, and ThT assay), V.G. (genetic analyses and plasmid designs), W.M. (MALDI imaging, MS, and LCO stainings), G.G. (cell transfection and immunoblotting with protease inhibitors and CTF fragments), M.Z. (transmission electron microscopy), L.S. (SEC), and S.A.M. (MS for APPUpp cleavage site determination of transfected cell culture). M.P.d.l.V., V.G., W.M., T.D., L.S., I.A., L.N.G.N., A.E., D.W., G.F.S., J.H., S.F.L., L.L., D.S., and M.I. analyzed the data. L.K., R.B., M.L., and M.I. contributed to sample collection. M.P.d.l.V., V.G., D.S., and M.I. wrote the first draft of the paper. All authors contributed to the final version of the paper. **Competing interests:** L.N.G.N. has received an honorarium from BioArctic AB and has a research collaboration with this company, outside the submitted work. L.L. is a cofounder of BioArctic AB. M.I. is a paid consultant for BioArctic AB. **Data and materials availability:** All data associated with this study are present in the paper or the Supplementary Materials. Materials in this study will be made available by contacting the corresponding author and completion of a material transfer agreement. Exon 17 nucleotide sequence for Uppsala mutation was submitted to GenBank (MW892394). Density maps of the AβUpp1–42$_{\Delta 19–24}$ obtained by cryo-EM were deposited in the EMDB for polymorph 1 (EMD-12592) and for polymorph 2 (EMD-12593).

Submitted 5 May 2020
Resubmitted 5 February 2021
Accepted 22 June 2021
Published 11 August 2021
10.1126/scitranslmed.abc6184

Citation: M. Pagnon de la Vega, V. Giedraitis, W. Michno, L. Kilander, G. Güner, M. Zielinski, M. Löwenmark, R. Brundin, T. Danfors, L. Söderberg, I. Alafuzoff, L. N. Nilsson, A. Erlandsson, D. Willbold, S. A. Müller, G. F. Schröder, J. Hanrieder, S. F. Lichtenthaler, L. Lannfelt, D. Sehlin, M. Ingelsson, The *Uppsala APP* deletion causes early onset autosomal dominant Alzheimer's disease by altering APP processing and increasing amyloid β fibril formation. *Sci. Transl. Med.* **13**, eabc6184 (2021).